Cite as: M. D. Kornberg *et al.*, *Science* 10.1126/science.aan4665 (2018).

Dimethyl fumarate targets GAPDH and aerobic glycolysis to modulate immunity

Michael D. Kornberg,[1] Pavan Bhargava,[1] Paul M. Kim,[2] Vasanta Putluri,[3] Adele M. Snowman,[4] Nagireddy Putluri,[3,5] Peter A. Calabresi,[1,4] Solomon H. Snyder[2,4,6]*

[1]Department of Neurology, Johns Hopkins University School of Medicine, Baltimore, MD 21287, USA. [2]Department of Psychiatry and Behavioral Sciences, Johns Hopkins University School of Medicine, Baltimore, MD 21287, USA. [3]Advanced Technology Core, Baylor College of Medicine, Houston, TX 77030, USA. [4]Department of Neuroscience, Johns Hopkins University School of Medicine, Baltimore, MD 21205, USA. [5]Department of Molecular and Cellular Biology, Baylor College of Medicine, Houston, TX 77030, USA. [6]Department of Pharmacology and Molecular Sciences, Johns Hopkins University School of Medicine, Baltimore, MD 21205, USA.

*Corresponding author. Email: ssnyder@jhmi.edu

Activated immune cells undergo a metabolic switch to aerobic glycolysis akin to the Warburg effect, presenting a potential therapeutic target in autoimmune disease. Dimethyl fumarate, a derivative of the Krebs cycle intermediate fumarate, is an immunomodulatory drug used to treat multiple sclerosis and psoriasis. Although its therapeutic mechanism remains uncertain, it covalently modifies cysteine residues in a process termed "succination." Here, we show that dimethyl fumarate succinates and inactivates the catalytic cysteine of the glycolytic enzyme GAPDH both in vitro and in vivo. It thereby downregulates aerobic glycolysis in activated myeloid and lymphoid cells, which mediates its anti-inflammatory effects. Our findings provide mechanistic insight into immune modulation by dimethyl fumarate and represent a proof of concept that aerobic glycolysis is a therapeutic target in autoimmunity.

Pro-inflammatory stimuli induce a metabolic switch in both myeloid and lymphoid cells, leading to a Warburg-like upregulation of aerobic glycolysis that regulates the balance between inflammatory and regulatory immune phenotypes (*1*, *2*). Classically activated macrophages and effector lymphocytes such as T-helper (Th) 1 and Th17 cells require glycolysis for their survival, differentiation, and effector functions (*3*–*9*), whereas oxidative metabolism favors the differentiation of alternatively activated (M2) macrophages and regulatory T (Treg) cells (*10*, *11*).

Dimethyl fumarate (DMF) is a serendipitously discovered immunomodulatory drug used to treat psoriasis and multiple sclerosis (MS) (*12*). Although its mechanisms of action remain incompletely understood, it is known to covalently modify cysteine residues in a process termed "succination" (not to be confused with lysine succinylation) (fig. S1) (*13*, *14*). DMF succinates kelch-like ECH-associated protein 1 (KEAP1), which activates nuclear factor (erythroid-derived 2)-related factor 2 (Nrf2) to produce anti-oxidant and anti-inflammatory effects that nonetheless fail to fully account for the drug's actions (*15*). Endogenous fumarate also succinates proteins, with a primary target being the active-site cysteine of the glycolytic enzyme glyceraldehyde 3-phosphate dehydrogenase (GAPDH) (*16*). In this study, we show that DMF and its clinically relevant metabolite monomethyl fumarate (MMF) target GAPDH and inactivate its enzyme activity, both in vitro and after oral treatment in mice and humans. In turn, GAPDH inhibition downregulates aerobic glycolysis in myeloid and lymphoid cells, preventing immune activation and shifting the balance between inflammatory and regulatory cell types.

To determine whether GAPDH was succinated by DMF and MMF, we performed liquid chromatography–tandem mass spectrometry (LC–MS/MS). Treatment of recombinant human GAPDH with MMF led to monomethyl succination (2-monomethyl succinyl-cysteine) at its active-site cysteine (Cys-152 in human) and cysteines 156 and 247, whereas DMF produced a combination of dimethyl (2-dimethyl succinyl-cysteine) and monomethyl succination at the same cysteines (table S1 and fig. S2). Neither of these modifications was observed at any cysteine in vehicle-treated GAPDH. In mice, oral treatment with DMF led to both monomethyl and dimethyl succination exclusively of the active-site cysteine (Cys-150 in mouse) of GAPDH purified from the spleen and brain, with no such modifications observed on other cysteines or in vehicle-treated mice (Fig. 1A and table S1). Although only the monomethyl form of the drug is detected in serum (*17*), our finding that dimethyl succination occurred after oral administration was consistent with prior work (*18*, *19*). Monomethyl succination of GAPDH Cys-152 was also identified in peripheral blood mononuclear cells (PBMCs) from MS patients treated with DMF (Fig. 1B and table S1) but not on other cysteines or in PBMCs from MS patients not treated with DMF. GAPDH succination by endogenous fumarate occurred physiologically, as we identified modification by fumarate (2-succinyl-

cysteine) at the active-site cysteine in vehicle-treated mice and human healthy controls (fig. S3).

Covalent modification of its catalytic cysteine should irreversibly inactivate GAPDH. We found that both DMF and MMF decreased the catalytic activity of recombinant GAPDH in a dose- and time-dependent manner (Fig. 1C). This inhibition was irreversible, as desalting failed to restore activity (fig. S4A). Additionally, this inhibition was mediated by active-site binding of DMF/MMF, as the drug effect was blocked by pre-incubation with tenfold excess of GAPDH substrates (fig. S4B). GAPDH inhibition was biphasic, with an initial fast phase and a secondary slow phase. We calculated the kinetics of inhibition for both phases using the Kitz–Wilson method (*20*) (fig. S4C). GAPDH activity was similarly inhibited in cultured mouse peritoneal macrophages (mPMs) treated overnight with 25 μM DMF (Fig. 1D). In mice, oral treatment with DMF decreased GAPDH activity measured from both the spleen and small intestine (Fig. 1E). This effect was particularly profound in the small intestine, which may be relevant given the role of the gut immune system in autoimmune disorders such as MS (*21*).

We next asked whether GAPDH inhibition by DMF impacted aerobic glycolysis in activated immune cells. Using lactate production as a proxy measure, co-treatment with DMF significantly impaired glycolysis in mPMs stimulated in vitro for 24 hours with 1 μg/ml lipopolysaccharide (LPS) (Fig. 2A). MMF had a similar effect but with lower potency. The influence on glycolysis was not due to cytotoxicity (fig. S5). Measurements of the extracellular acidification rate (ECAR) revealed a similar inhibition of aerobic glycolysis by DMF and MMF in LPS-stimulated mPMs (Fig. 2B). In activated mouse and human $CD4^+$ lymphocytes, DMF and MMF decreased basal glycolysis, with an even greater effect on maximal glycolytic capacity (Fig. 2C and fig. S6). In LPS-stimulated mPMs, treatment with DMF produced a blockade in glycolytic flux at GAPDH (Fig. 2D and fig. S7), providing evidence that GAPDH inactivation mediated the downregulation of glycolysis by DMF.

DMF had no effect on glycolysis in unstimulated mPMs (Fig. 2E), raising the possibility that DMF acts not only on GAPDH but also on the signaling pathway required for glycolytic upregulation. However, DMF had no effect on the activity of mechanistic target of rapamycin (mTOR, as measured via p70-S6 kinase phosphorylation) or levels of hypoxia-inducible factor 1-α (HIF-1α) (Fig. 2F and fig. S8). This selective inhibition of glycolysis in LPS-stimulated mPMs is consistent with recent evidence that GAPDH only becomes a rate-limiting enzyme when glycolysis is upregulated in the setting of Warburg physiology (*22–24*), as it is in cancer and activated immune cells. This likely explains why DMF is not generally toxic.

We also examined whether DMF impacted oxidative phosphorylation (OXPHOS). DMF increased OXPHOS in mPMs under both resting and LPS-stimulated conditions (fig. S9A). The inhibition of glycolysis did not depend on the upregulation of OXPHOS (fig. S9, B and C).

We next asked whether inhibition of GAPDH and aerobic glycolysis mediated the immunologic actions of DMF. We first addressed this question in macrophages. We reproduced previous findings that both DMF and glycolytic blockade prevent classical macrophage activation (fig. S10, A to D) (*3*, *25*) and then determined that the inhibition of cytokine production by DMF was unrelated to its effects on OXPHOS (fig. S10E). We next measured the production of IL-1β under low (0.5 mM) or high (10 mM) glucose concentrations and found that DMF was much less effective in the presence of high glucose (Fig. 3A), suggesting that its anti-inflammatory effect can be overcome by driving glycolysis higher with saturating concentrations of glucose. DMF augmented the IL-4-induced expression of arginase-1 (Arg-1), a marker of M2 alternative activation (fig. S10F), but the relative importance of DMF effects on aerobic glycolysis versus OXPHOS in promoting alternative activation was not examined.

Heptelidic acid (also known as koningic acid) is a GAPDH inhibitor, which binds the active site and covalently modifies the catalytic cysteine (*23*, *26*). The treatment of mPMs with heptelidic acid replicated the effects of DMF on IL-1β secretion (Fig. 3B), inducible nitric oxide synthase (iNOS) expression (Fig. 3C and fig. S11A), and nuclear translocation of nuclear factor-κB (NF- κB) (Fig. 3D and fig. S11B). Conversely, the overexpression of wild-type GAPDH, but not catalytically inactive GAPDH mutated at Cys-150, mitigated the effect of DMF on IL-1β production (Fig. 3E and fig. S12). Thus, the immunologic actions of DMF were replicated by GAPDH inhibition and reversed by increasing GAPDH expression.

We next examined the effects of DMF and MMF on lymphocyte differentiation and function. We activated mouse naïve $CD4^+$ T cells under Th1-, Th17-, or Treg-cell-polarizing conditions for four days ± DMF or MMF, with treatment at the start of polarization. Consistent with known effects of glycolytic blockade (*7*, *8*), DMF disproportionately impacted the survival of Th1 and Th17 versus Treg cells (Fig. 4A and fig. S13A). Similarly, DMF/MMF inhibited both differentiation and cytokine production under Th1- and Th17-polarizing conditions, an effect replicated by heptelidic acid (Fig. 4, B to D, and fig. S13B). As reported with HIF-1α deficiency and 2-deoxyglucose (*11*), DMF promoted Treg-cell differentiation under Treg-polarizing conditions (Fig. 4E and fig. S13B), and both DMF and MMF reciprocally inhibited Th17 and promoted Treg cell development under Th17-polarizing conditions (Fig. 4F). When added after three days of polarization, DMF, MMF, and low-dose heptelidic

acid had no effect on viability (fig. S14A) or differentiation (fig. S14B) of Th1 or Th17 cells. However, all three drugs inhibited the expression of IFNγ and IL-17 (Fig. 4G), suggesting an effect on cytokine production independent of survival and differentiation.

Because GAPDH binding to mRNA underlies post-transcriptional regulation of cytokine production (*9*), we tested the effect of GAPDH succination on RNA binding (fig. S15). Pre-treatment with DMF (or heptelidic acid) decreased GAPDH–RNA binding, as reported with other modifications of the active-site cysteine (*27*). This effect was small, however, as a similar decrease was produced by a tenfold lower concentration of NAD^+. Thus, the alteration of such binding does not appear to underlie the immunologic actions of DMF.

Finally, to ascertain whether GAPDH inhibition produced anti-inflammatory actions in vivo, we examined the effect of heptelidic acid in experimental autoimmune encephalomyelitis (EAE), a mouse model of MS, and found that it attenuated the disease in these mice (Fig. 4H).

By demonstrating that a known immunomodulatory drug acts by inhibiting aerobic glycolysis, our findings provide a proof of concept that metabolism is a viable therapeutic target in autoimmunity. They may also explain important observations of DMF therapy in patients. DMF differentially impacts distinct lymphocyte subsets, producing lymphopenia that selectively depletes highly glycolytic effector T cells while sparing oxidative naïve T cells and Treg cells (*28*, *29*). Our findings suggest that the inhibition of aerobic glycolysis underlies these selective effects. It is also notable that DMF is simply a derivative of fumarate, which is a metabolic intermediate of the Krebs cycle, lying downstream of glycolysis in cellular energy production. We hypothesize that fumarate-induced inactivation of GAPDH represents an endogenous negative feedback loop. DMF—a more cell-permeable and electrophilic derivative of fumarate—may simply exploit this physiologic pathway to produce its immunologic actions (Fig. 4I). It must be noted, however, that additional targets of succination (in addition to KEAP1) are likely relevant to both the therapeutic and toxic effects of the drug.

REFERENCES AND NOTES

1. E. L. Pearce, E. J. Pearce, Metabolic pathways in immune cell activation and quiescence. *Immunity* **38**, 633–643 (2013). doi:10.1016/j.immuni.2013.04.005 Medline

2. B. Kelly, L. A. O'Neill, Metabolic reprogramming in macrophages and dendritic cells in innate immunity. *Cell Res.* **25**, 771–784 (2015). doi:10.1038/cr.2015.68 Medline

3. G. M. Tannahill, A. M. Curtis, J. Adamik, E. M. Palsson-McDermott, A. F. McGettrick, G. Goel, C. Frezza, N. J. Bernard, B. Kelly, N. H. Foley, L. Zheng, A. Gardet, Z. Tong, S. S. Jany, S. C. Corr, M. Haneklaus, B. E. Caffrey, K. Pierce, S. Walmsley, F. C. Beasley, E. Cummins, V. Nizet, M. Whyte, C. T. Taylor, H. Lin, S. L. Masters, E. Gottlieb, V. P. Kelly, C. Clish, P. E. Auron, R. J. Xavier, L. A. J. O'Neill, Succinate is an inflammatory signal that induces IL-1β through HIF-1α. *Nature* **496**, 238–242 (2013). doi:10.1038/nature11986 Medline

4. C. M. Cham, T. F. Gajewski, Glucose availability regulates IFN-γ production and p70S6 kinase activation in $CD8^+$ effector T cells. *J. Immunol.* **174**, 4670–4677 (2005). doi:10.4049/jimmunol.174.8.4670 Medline

5. C. M. Cham, G. Driessens, J. P. O'Keefe, T. F. Gajewski, Glucose deprivation inhibits multiple key gene expression events and effector functions in $CD8^+$ T cells. *Eur. J. Immunol.* **38**, 2438–2450 (2008). doi:10.1002/eji.200838289 Medline

6. R. Wang, C. P. Dillon, L. Z. Shi, S. Milasta, R. Carter, D. Finkelstein, L. L. McCormick, P. Fitzgerald, H. Chi, J. Munger, D. R. Green, The transcription factor Myc controls metabolic reprogramming upon T lymphocyte activation. *Immunity* **35**, 871–882 (2011). doi:10.1016/j.immuni.2011.09.021 Medline

7. A. N. Macintyre, V. A. Gerriets, A. G. Nichols, R. D. Michalek, M. C. Rudolph, D. Deoliveira, S. M. Anderson, E. D. Abel, B. J. Chen, L. P. Hale, J. C. Rathmell, The glucose transporter Glut1 is selectively essential for CD4 T cell activation and effector function. *Cell Metab.* **20**, 61–72 (2014). doi:10.1016/j.cmet.2014.05.004 Medline

8. V. A. Gerriets, R. J. Kishton, A. G. Nichols, A. N. Macintyre, M. Inoue, O. Ilkayeva, P. S. Winter, X. Liu, B. Priyadharshini, M. E. Slawinska, L. Haeberli, C. Huck, L. A. Turka, K. C. Wood, L. P. Hale, P. A. Smith, M. A. Schneider, N. J. MacIver, J. W. Locasale, C. B. Newgard, M. L. Shinohara, J. C. Rathmell, Metabolic programming and PDHK1 control $CD4^+$ T cell subsets and inflammation. *J. Clin. Invest.* **125**, 194–207 (2015). doi:10.1172/JCI76012 Medline

9. C. H. Chang, J. D. Curtis, L. B. Maggi Jr., B. Faubert, A. V. Villarino, D. O'Sullivan, S. C.-C. Huang, G. J. W. van der Windt, J. Blagih, J. Qiu, J. D. Weber, E. J. Pearce, R. G. Jones, E. L. Pearce, Posttranscriptional control of T cell effector function by aerobic glycolysis. *Cell* **153**, 1239–1251 (2013). doi:10.1016/j.cell.2013.05.016 Medline

10. D. Vats, L. Mukundan, J. I. Odegaard, L. Zhang, K. L. Smith, C. R. Morel, R. A. Wagner, D. R. Greaves, P. J. Murray, A. Chawla, Oxidative metabolism and PGC-1β attenuate macrophage-mediated inflammation. *Cell Metab.* **4**, 13–24 (2006). doi:10.1016/j.cmet.2006.05.011 Medline

11. L. Z. Shi, R. Wang, G. Huang, P. Vogel, G. Neale, D. R. Green, H. Chi, HIF1α-dependent glycolytic pathway orchestrates a metabolic checkpoint for the differentiation of T_H17 and T_{reg} cells. *J. Exp. Med.* **208**, 1367–1376 (2011). doi:10.1084/jem.20110278 Medline

12. R. A. Linker, A. Haghikia, Dimethyl fumarate in multiple sclerosis: Latest developments, evidence and place in therapy. *Ther. Adv. Chronic Dis.* **7**, 198–207 (2016). doi:10.1177/2040622316653307 Medline

13. R. A. Linker, D.-H. Lee, S. Ryan, A. M. van Dam, R. Conrad, P. Bista, W. Zeng, X. Hronowsky, A. Buko, S. Chollate, G. Ellrichmann, W. Brück, K. Dawson, S. Goelz, S. Wiese, R. H. Scannevin, M. Lukashev, R. Gold, Fumaric acid esters exert neuroprotective effects in neuroinflammation via activation of the Nrf2 antioxidant pathway. *Brain* **134**, 678–692 (2011). doi:10.1093/brain/awq386 Medline

14. M. M. Blewett, J. Xie, B. W. Zaro, K. M. Backus, A. Altman, J. R. Teijaro, B. F. Cravatt, Chemical proteomic map of dimethyl fumarate-sensitive cysteines in primary human T cells. *Sci. Signal.* **9**, rs10 (2016). doi:10.1126/scisignal.aaf7694 Medline

15. U. Schulze-Topphoff, M. Varrin-Doyer, K. Pekarek, C. M. Spencer, A. Shetty, S. A. Sagan, B. A. C. Cree, R. A. Sobel, B. T. Wipke, L. Steinman, R. H. Scannevin, S. S. Zamvil, Dimethyl fumarate treatment induces adaptive and innate immune modulation independent of Nrf2. *Proc. Natl. Acad. Sci. U.S.A.* **113**, 4777–4782 (2016). doi:10.1073/pnas.1603907113 Medline

16. M. Blatnik, N. Frizzell, S. R. Thorpe, J. W. Baynes, Inactivation of glyceraldehyde-3-phosphate dehydrogenase by fumarate in diabetes: Formation of S-(2-succinyl)cysteine, a novel chemical modification of protein and possible biomarker of mitochondrial stress. *Diabetes* **57**, 41–49 (2008). doi:10.2337/db07-0838 Medline

17. N. H. Litjens, J. Burggraaf, E. van Strijen, C. van Gulpen, H. Mattie, R. C. Schoemaker, J. T. van Dissel, H. B. Thio, P. H. Nibbering, Pharmacokinetics of oral fumarates in healthy subjects. *Br. J. Clin. Pharmacol.* **58**, 429–432 (2004). doi:10.1111/j.1365-2125.2004.02145.x Medline

18. M. Rostami-Yazdi, B. Clement, T. J. Schmidt, D. Schinor, U. Mrowietz, Detection of metabolites of fumaric acid esters in human urine: Implications for their mode of action. *J. Invest. Dermatol.* **129**, 231–234 (2009). doi:10.1038/jid.2008.197 Medline

19. H. Peng, H. Li, A. Sheehy, P. Cullen, N. Allaire, R. H. Scannevin, Dimethyl fumarate alters microglia phenotype and protects neurons against proinflammatory toxic microenvironments. *J. Neuroimmunol.* **299**, 35–44 (2016). doi:10.1016/j.jneuroim.2016.08.006 Medline

20. Z. D. Parsons, K. S. Gates, Redox regulation of protein tyrosine phosphatases: Methods for kinetic analysis of covalent enzyme inactivation. *Methods Enzymol.* **528**, 129–154 (2013). doi:10.1016/B978-0-12-405881-1.00008-2

21. N. Kamada, S. U. Seo, G. Y. Chen, G. Núñez, Role of the gut microbiota in immunity and inflammatory disease. *Nat. Rev. Immunol.* **13**, 321–335 (2013). doi:10.1038/nri3430 Medline

22. A. A. Shestov, X. Liu, Z. Ser, A. A. Cluntun, Y. P. Hung, L. Huang, D. Kim, A. Le, G. Yellen, J. G. Albeck, J. W. Locasale, Quantitative determinants of aerobic glycolysis identify flux through the enzyme GAPDH as a limiting step. *eLife* **3**, 03342 (2014). Medline

23. M. V. Liberti, Z. Dai, S. E. Wardell, J. A. Baccile, X. Liu, X. Gao, R. Baldi, M. Mehrmohamadi, M. O. Johnson, N. S. Madhukar, A. A. Shestov, I. I. C. Chio, O. Elemento, J. C. Rathmell, F. C. Schroeder, D. P. McDonnell, J. W. Locasale, A predictive model for selective targeting of the Warburg effect through GAPDH inhibition with a natural product. *Cell Metab.* **26**, 648–659.e8 (2017). doi:10.1016/j.cmet.2017.08.017 Medline

24. J. Yun, E. Mullarky, C. Lu, K. N. Bosch, A. Kavalier, K. Rivera, J. Roper, I. I. C. Chio, E. G. Giannopoulou, C. Rago, A. Muley, J. M. Asara, J. Paik, O. Elemento, Z. Chen, D. J. Pappin, L. E. Dow, N. Papadopoulos, S. S. Gross, L. C. Cantley, Vitamin C selectively kills KRAS and BRAF mutant colorectal cancer cells by targeting GAPDH. *Science* **350**, 1391–1396 (2015). doi:10.1126/science.aaa5004 Medline

25. M. A. Michell-Robinson, C. S. Moore, L. M. Healy, L. A. Osso, N. Zorko, V. Grouza, H. Touil, L. Poliquin-Lasnier, A.-M. Trudelle, P. S. Giacomini, A. Bar-Or, J. P. Antel, Effects of fumarates on circulating and CNS myeloid cells in multiple sclerosis. *Ann. Clin. Transl. Neurol.* **3**, 27–41 (2015). doi:10.1002/acn3.270 Medline

26. K. Sakai, K. Hasumi, A. Endo, Identification of koningic acid (heptelidic acid)-modified site in rabbit muscle glyceraldehyde-3-phosphate dehydrogenase. *Biochim. Biophys. Acta* **1077**, 192–196 (1991). doi:10.1016/0167-4838(91)90058-8 Medline

27. E. Nagy, W. F. Rigby, Glyceraldehyde-3-phosphate dehydrogenase selectively binds AU-rich RNA in the NAD^+-binding region (Rossmann fold). *J. Biol. Chem.* **270**, 2755–2763 (1995). doi:10.1074/jbc.270.6.2755 Medline

28. C. M. Spencer, E. C. Crabtree-Hartman, K. Lehmann-Horn, B. A. Cree, S. S. Zamvil, Reduction of $CD8^+$ T lymphocytes in multiple sclerosis patients treated with dimethyl fumarate. *Neurol. Neuroimmunol. Neuroinflamm.* **2**, e76 (2015). doi:10.1212/NXI.0000000000000076 Medline

29. C. C. Gross, A. Schulte-Mecklenbeck, S. Klinsing, A. Posevitz-Fejfár, H. Wiendl, L. Klotz, Dimethyl fumarate treatment alters circulating T helper cell subsets in multiple sclerosis. *Neurol. Neuroimmunol. Neuroinflamm.* **3**, e183 (2015). doi:10.1212/NXI.0000000000000183 Medline

30. M. R. Hara, N. Agrawal, S. F. Kim, M. B. Cascio, M. Fujimuro, Y. Ozeki, M. Takahashi, J. H. Cheah, S. K. Tankou, L. D. Hester, C. D. Ferris, S. D. Hayward, S. H. Snyder, A. Sawa, S-nitrosylated GAPDH initiates apoptotic cell death by nuclear translocation following Siah1 binding. *Nat. Cell Biol.* **7**, 665–674 (2005). doi:10.1038/ncb1268 Medline

31. P. A. Calabresi, R. Allie, K. M. Mullen, S. H. Yun, R. W. Georgantas 3rd, K. A. Whartenby, Kinetics of CCR7 expression differ between primary activation and effector memory states of T_H1 and T_H2 cells. *J. Neuroimmunol.* **139**, 58–65 (2003). doi:10.1016/S0165-5728(03)00127-9 Medline

32. A. Shevchenko, O. N. Jensen, A. V. Podtelejnikov, F. Sagliocco, M. Wilm, O. Vorm, P. Mortensen, A. Shevchenko, H. Boucherie, M. Mann, Linking genome and proteome by mass spectrometry: Large-scale identification of yeast proteins from two dimensional gels. *Proc. Natl. Acad. Sci. U.S.A.* **93**, 14440–14445 (1996). doi:10.1073/pnas.93.25.14440 Medline

33. A. Keller, A. I. Nesvizhskii, E. Kolker, R. Aebersold, Empirical statistical model to estimate the accuracy of peptide identifications made by MS/MS and database search. *Anal. Chem.* **74**, 5383–5392 (2002). doi:10.1021/ac025747h Medline

34. A. I. Nesvizhskii, A. Keller, E. Kolker, R. Aebersold, A statistical model for identifying proteins by tandem mass spectrometry. *Anal. Chem.* **75**, 4646–4658 (2003). doi:10.1021/ac0341261 Medline

35. G. J. van der Windt, C. H. Chang, E. L. Pearce. Measuring bioenergetics in T cells using a Seahorse extracellular flux analyzer. *Curr. Protoc. Immunol.* **113**, 16B.1-16B.14 (2016).

36. V. Vantaku, S. R. Donepudi, C. R. Ambati, F. Jin, V. Putluri, K. Nguyen, K. Rajapakshe, C. Coarfa, V. L. Battula, Y. Lotan, N. Putluri, Expression of ganglioside GD2, reprogram the lipid metabolism and EMT phenotype in bladder cancer. *Oncotarget* **8**, 95620–95631 (2017). doi:10.18632/oncotarget.21038 Medline

37. F. Jin, J. Thaiparambil, S. R. Donepudi, V. Vantaku, D. W. B. Piyarathna, S. Maity, R. Krishnapuram, V. Putluri, F. Gu, P. Purwaha, S. K. Bhowmik, C. R. Ambati, F.-C. von Rundstedt, F. Roghmann, S. Berg, J. Noldus, K. Rajapakshe, D. Gödde, S. Roth, S. Störkel, S. Degener, G. Michailidis, B. A. Kaipparettu, B. Karanam, M. K. Terris, S. M. Kavuri, S. P. Lerner, F. Kheradmand, C. Coarfa, A. Sreekumar, Y. Lotan, R. El-Zein, N. Putluri, Tobacco-specific carcinogens induce hypermethylation, DNA adducts, and DNA damage in bladder cancer. *Cancer Prev. Res.* **10**, 588–597 (2017). doi:10.1158/1940-6207.CAPR-17-0198 Medline

38. D. W. B. Piyarathna, T. M. Rajendiran, V. Putluri, V. Vantaku, T. Soni, F. C. von Rundstedt, S. R. Donepudi, F. Jin, S. Maity, C. R. Ambati, J. Dong, D. Gödde, S. Roth, S. Störkel, S. Degener, G. Michailidis, S. P. Lerner, S. Pennathur, Y. Lotan, C. Coarfa, A. Sreekumar, N. Putluri, Distinct lipidomic landscapes associated with clinical stages of urothelial cancer of the bladder. *Eur. Urol. Focus* **17**, 30107–30114 (2017). Medline

ACKNOWLEDGMENTS

We thank J. Liu and J. Stivers for insights regarding enzyme kinetics experiments. We are grateful to Z. Zhou, W. Chen, and A. Hoke for providing access to the Seahorse extracellular flux analyzer and support with its use. We thank L. DeVine and R. Cole from the Johns Hopkins Mass Spectrometry Core Facility for their assistance and helpful discussion. We are grateful to B. Wipke and R. Scannevin for insightful discussion and for providing a protocol for preparation of DMF suspension. We thank B. Paul for help with mPM isolation and GAPDH–RNA binding, C. Darius for drawing blood samples, and J. Bo for preparation of PBMCs. **Funding:** Funding for M.D.K. was provided by the NINDS (R25 grant, RFA-NS-12-003), National Multiple Sclerosis Society (NMSS) – American Academy of Neurology (AAN) (Clinician Scientist Development Award, FAN 17107-A-1), and Conrad N. Hilton Foundation (Marilyn Hilton Bridging Award). Funding for P.B. was provided by the AAN (John F. Kurtzke Clinician Scientist Development Award), NMSS (Career Transition Award, TA-1503-03465), and Race to Erase MS (Young Investigator Award). V.P. and N.P. were supported by the CPRIT Core Facility Support Award (RP170005), NCI Cancer Center Support Grant (P30CA125123), and intramural funds from the Dan L. Duncan Cancer

Center (DLDCC). N.P. was also supported by the American Cancer Society (127430-RSG-15-105-01-CNE) and NIH (R01CA220297 and R01CA216426). Funding for P.A.C. was provided by the NINDS (R37NS041435). Funding for S.H.S. was provided by USPHS grant MH18501. **Author contributions:** M.D.K., P.B., P.A.C, and S.H.S. contributed to overall project design. M.D.K., P.B., P.M.K., V.P., N.P., and A.M.S. performed the research. M.D.K., P.B., P.M.K., V.P., and N.P., analyzed the data. M.D.K. and P.B. prepared the figures. M.D.K. and S.H.S. wrote the manuscript. P.B., P.A.C., and N.P. edited the manuscript. **Competing interests:** P.A.C. has received research funding in the past from Biogen, the company that sells DMF (trade name Tecfidera) as a therapy for MS. He received a consulting honorarium from Biogen in 2015 for work related to the compound opicinumab. The other authors declare no competing interests. **Data and materials availability:** Data in this paper are presented and/or tabulated in the main text and supplementary materials.

SUPPLEMENTARY MATERIALS

www.sciencemag.org/cgi/content/full/science.aan4665/DC1
Materials and Methods
Table S1
Figs. S1 to S15
References (*30*–*38*)

27 April 2017; resubmitted 29 January 2018
Accepted 15 March 2018
Published online 29 March 2018
10.1126/science.aan4665

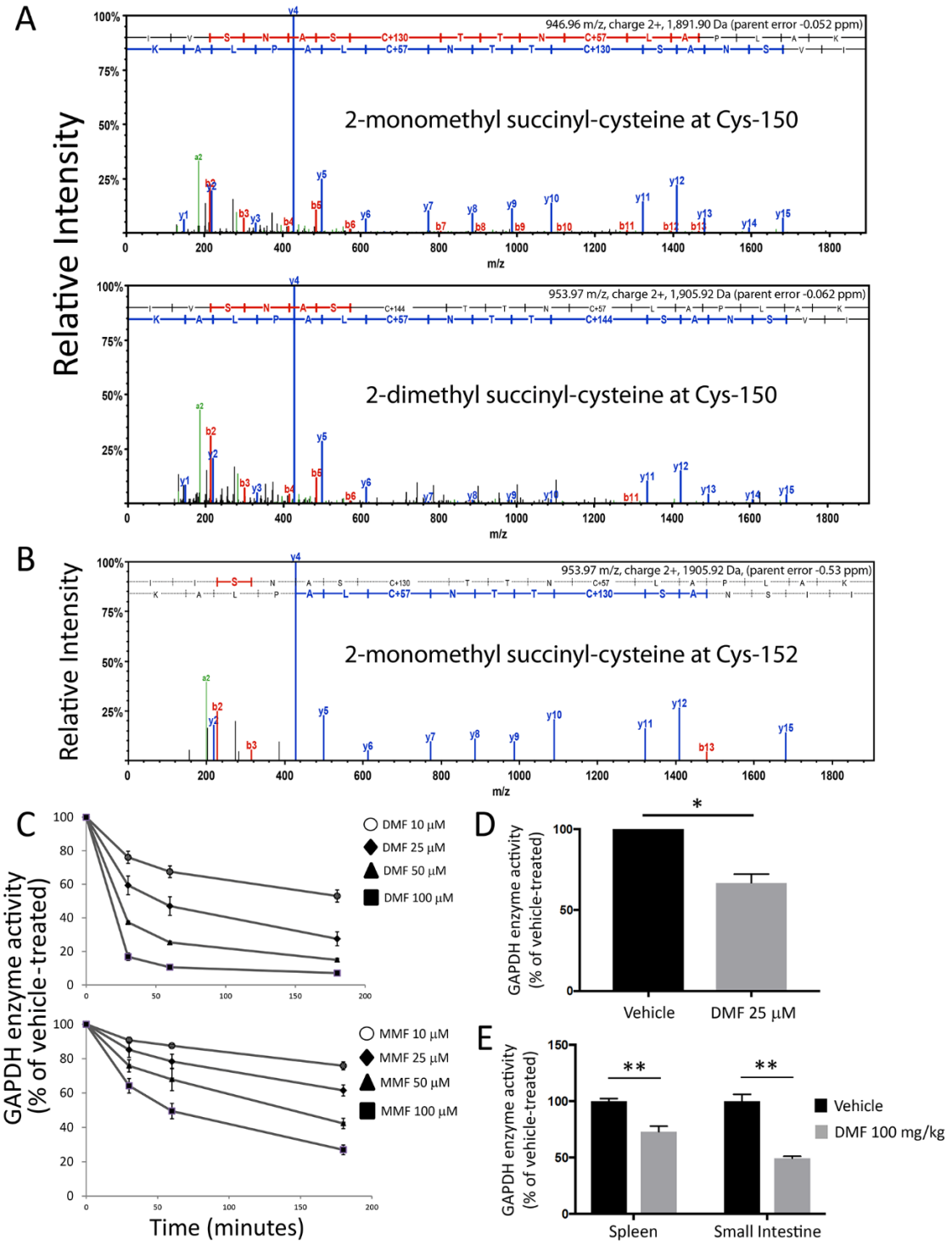

Fig. 1. DMF and MMF succinate and inactivate GAPDH in vitro and after oral treatment. (**A**) Representative LC-MS/MS spectra demonstrating covalent modification of the catalytic cysteine (Cys-150 in mouse) by either monomethyl (2-monomethyl succinyl-cysteine, +130 Da) or dimethyl (2-dimethyl succinyl-cysteine, +144 Da) fumarate in GAPDH immunoprecipitated from splenic lysates of mice treated orally with 100 mg/kg DMF daily for five days. Because samples were reduced and treated with iodoacetate, non-succinated cysteines were modified with carbamidomethyl (Carb, +57 Da). Pooled samples were analyzed from two vehicle-treated and two DMF-treated animals. (**B**) Representative LC-MS/MS spectrum demonstrating monomethyl succination of the catalytic cysteine (Cys-152 in human) of GAPDH immuno-precipitated from PBMC lysates of MS patients treated with DMF for three months. Pooled samples were analyzed from three DMF-treated and two non-DMF-treated patients. (**C**) Dose- and time-dependent inactivation of GAPDH enzyme activity in vitro. Recombinant GAPDH was treated with the indicated drug concentrations or vehicle alone. Aliquots were removed at the specified time points, followed by enzyme activity assay. Data were pooled from four experiments performed in duplicate and represent mean ± SEM for each time point. Associated Kitz–Wilson plots and kinetic parameters are shown in fig. S4C. (**D**) Peritoneal macrophages were treated overnight with DMF. Cells lysates were used for GAPDH enzyme activity assay. Data represent mean ± SEM of three experiments performed in duplicate. (**E**) Mice were treated with DMF 100 mg/kg daily for five days by oral gavage. On Day 5, mice were sacrificed, and lysates from spleen and small intestine were used for GAPDH enzyme activity assay. Data represent mean ± SEM of five mice per group, with assays run in triplicate. Da = daltons. $*P < 0.05$ and $**P < 0.01$ by two-tailed Student's *t*-test.

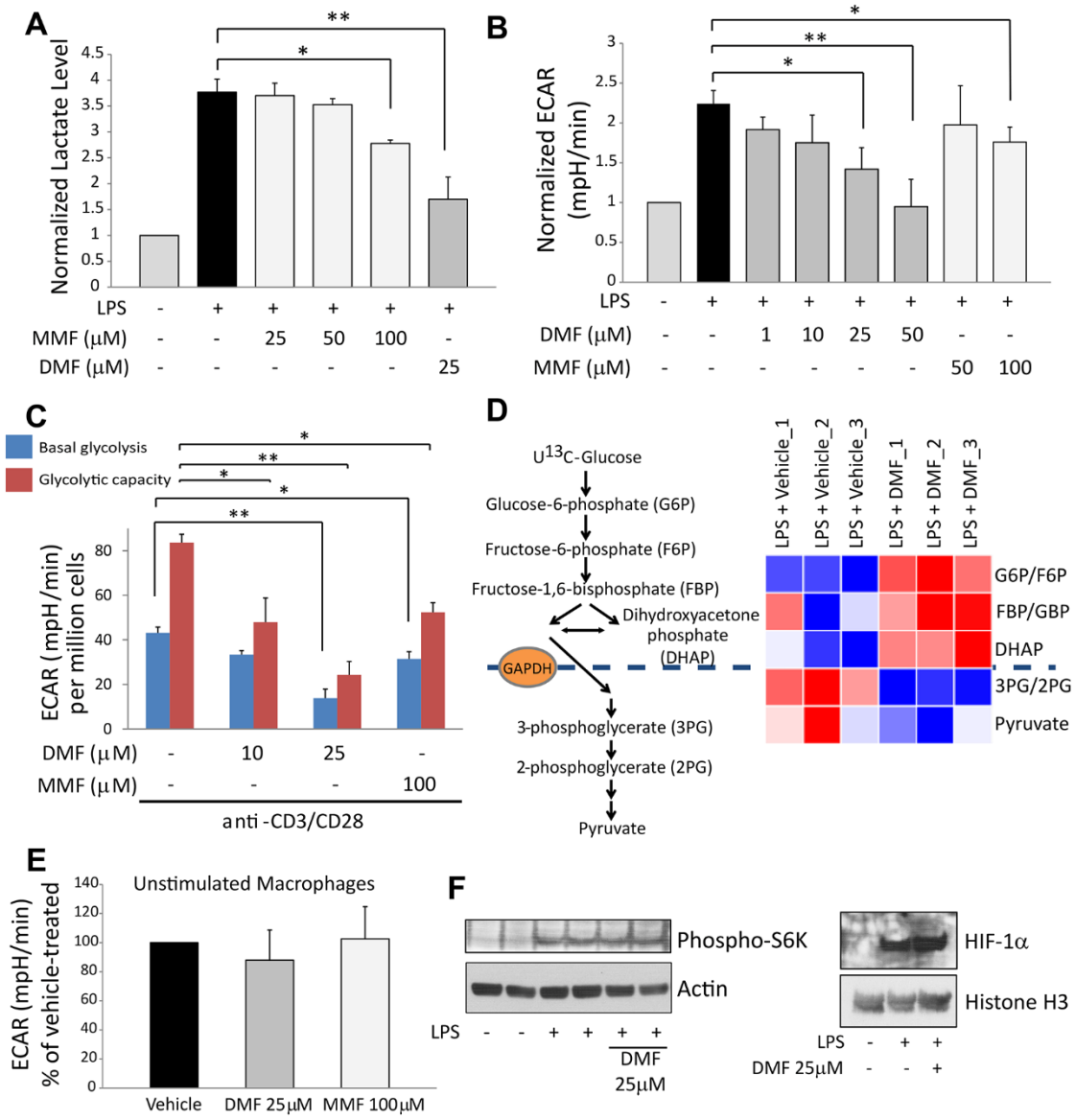

Fig. 2. GAPDH inactivation by DMF and MMF inhibits glycolysis in activated, but not resting, macrophages and lymphocytes. (**A**) Mouse peritoneal macrophages (mPMs) were treated with LPS ± DMF or MMF for 24 hours followed by measurement of lactate (a proxy measure of glycolysis) in culture media by colorimetric assay. Data represent mean ± SEM of three experiments performed in duplicate. (**B**) mPMs were treated as in (A), and glycolysis was measured as extracellular acidification rate (ECAR) using a Seahorse extracellular flux analyzer. Data represent mean ± SEM of five experiments performed in quadruplicate. (**C**) Glycolysis was measured via Seahorse extracellular flux analyzer in mouse naive $CD4^+$ lymphocytes activated overnight with anti-CD3/CD28 antibodies ± DMF/MMF. Data represent mean ± SEM of four experiments performed in triplicate. (**D**) mPMs were stimulated with LPS for 24 hours ± 25 μM DMF, in triplicate. Cells were then labeled with $U^{13}C$-glucose, and ^{13}C-labeling of glycolytic intermediates was measured from lysates via LC-MS. Heat map shows blockade of glycolytic flux at the level of GAPDH. (**E**) DMF/MMF had no effect on glycolysis in unstimulated mPMs, measured as ECAR. Data represent mean ± SEM of four experiments performed in quadruplicate. (**F**) Representative immunoblots showing no effect of DMF on phospho-S6K (a marker of mTOR activity) (*N* = two experiments performed in duplicate) or HIF-1α levels (*N* = three experiments) in LPS-stimulated mPMs. Data are quantified in fig. S8. $*P < 0.05$ and $**P < 0.01$ by one-way analysis of variance (ANOVA) with Dunnett's multiple comparison.

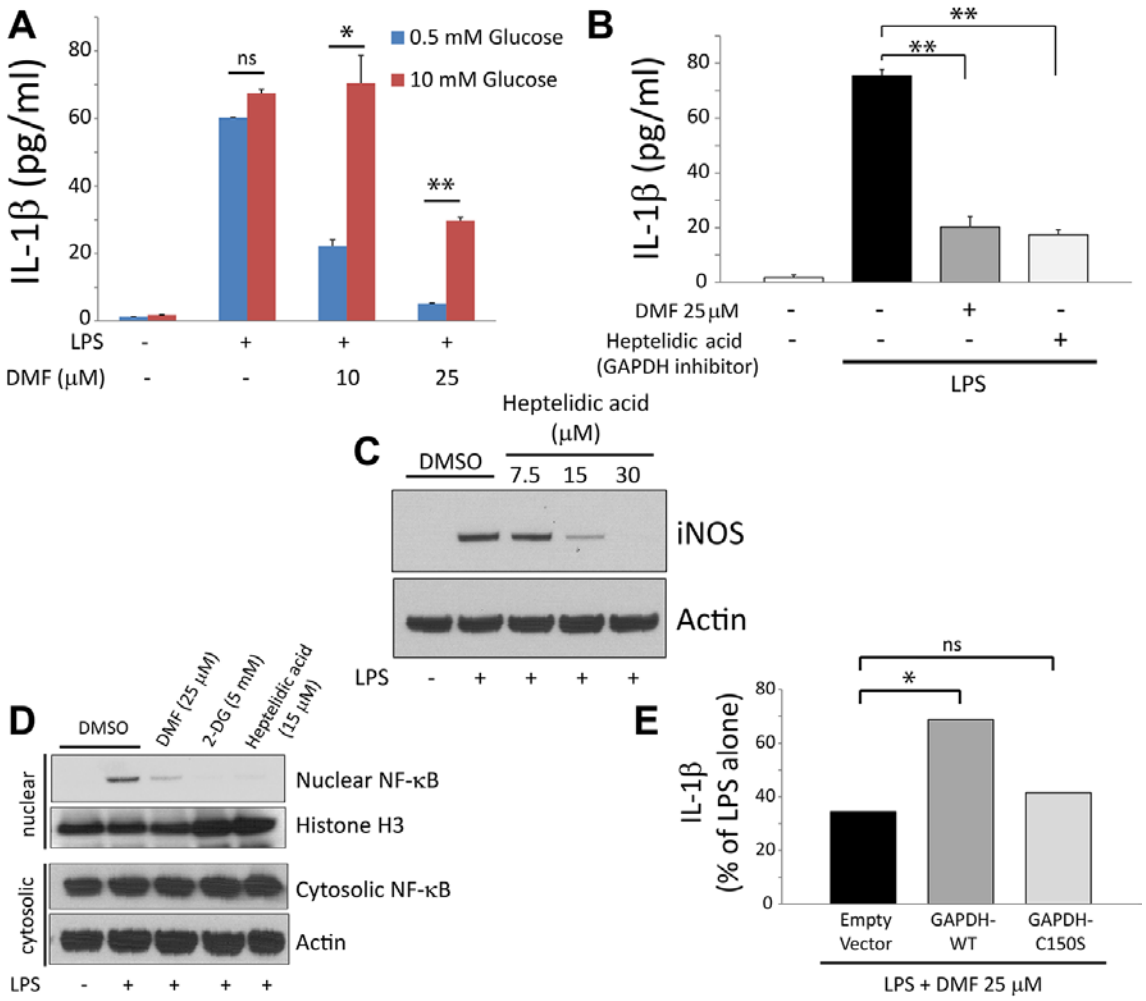

Fig. 3. Inhibition of GAPDH and aerobic glycolysis mediates anti-inflammatory effects of DMF in macrophages. (**A**) mPMs were treated with LPS ± DMF for 24 hours in either limiting (0.5 mM) or saturating (10 mM) concentrations of glucose, followed by measurement of IL-1β secretion by ELISA. Data represent mean ± SEM of three experiments performed in singlet or duplicate. (**B**) Treating LPS-stimulated mPMs with 30 μM heptelidic acid, a selective GAPDH inhibitor, replicated the effect of DMF on IL-1β secretion. Data represent mean ± SEM of three experiments performed in singlet or duplicate. (**C** and **D**) Representative immunoblots from three experiments showing that heptelidic acid replicated the effects of DMF on iNOS expression (C) and nuclear translocation of NF-κB (D) in LPS-stimulated mPMs. Data are quantified in fig. S11. (**E**) Overexpression of wild-type GAPDH (GAPDH-WT), but not Cys-150 mutant (GAPDH-C150S), mitigated the effect of DMF on IL-1β secretion in mPMs. Data represent the mean of two experiments performed in duplicate. ns = non-significant. **P* < 0.05 and ***P* < 0.01 by two-tailed Student's *t*-test (A) and one-way ANOVA with Dunnett's multiple comparison (B and E).

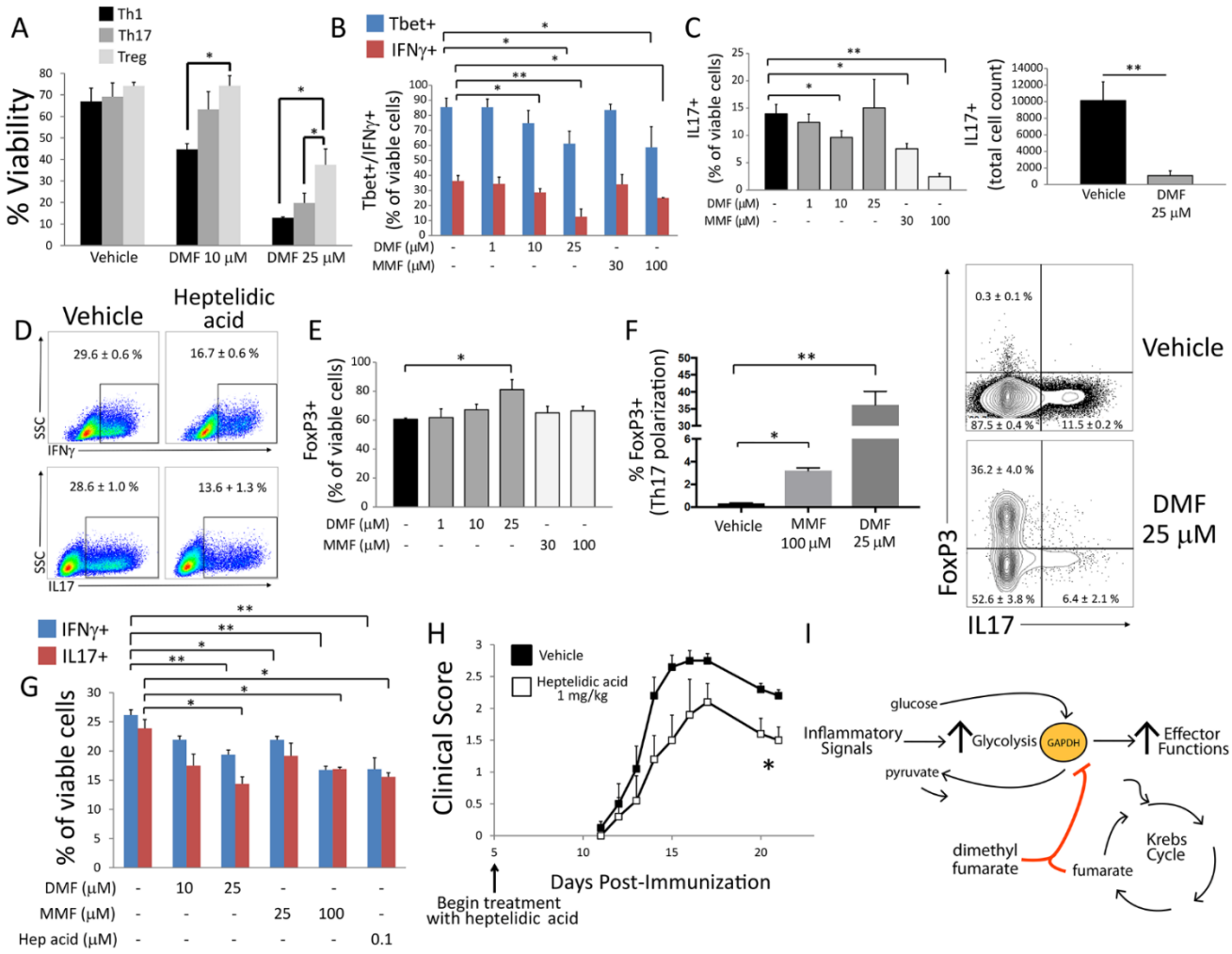

Fig. 4. DMF and MMF differentially impact survival, differentiation, and effector function of metabolically distinct lymphocyte subsets. (**A** to **F**) Mouse naïve CD4⁺ lymphocytes were activated for four days with anti-CD3/CD28 antibodies under Th1-, Th17-, or Treg-cell-polarizing conditions. Cells were treated with indicated doses of DMF, MMF, or heptelidic acid on day 0 and assayed by flow cytometry on day 4. (A) DMF disproportionately decreased survival under Th1- and Th17-cell vs. Treg-cell polarizing conditions, as assessed by LIVE/DEAD aqua stain. Data represent mean ± SEM of three experiments performed in duplicate or triplicate. (B and C) DMF/MMF decreased the proportion of Tbet⁺ and IFNγ⁺ cells under Th1-cell-polarizing conditions (B) and of IL-17⁺ cells under Th17-cell-polarizing conditions (C, left). DMF (25 μM) produced variable results under Th17-cell-polarizing conditions, likely due to high toxicity at that dose, but nonetheless caused a significant decrease in total IL-17⁺ cell count (C, right). Data represent mean ± SEM of three experiments performed in duplicate or triplicate. (D) Representative flow cytometric plots demonstrating that low-dose (0.5 μM) heptelidic acid replicated the effect of DMF/MMF on IFNγ and IL-17 expression under Th1- and Th17-cell-polarizing conditions, respectively. Toxicity limited the testing of higher doses. Values represent mean ± SEM of a triplicate experiment. (E) In contrast to effects on Th1 and Th17 cells, DMF increased the proportion of FoxP3⁺ cells under Treg-cell-polarizing conditions. Data represent mean ± SEM of three experiments performed in duplicate or triplicate. (F) DMF/MMF produced a reciprocal increase in FoxP3⁺ cells under Th17-cell-polarizing conditions. Bar graph (left) and representative flow cytometric plot (right) from a triplicate experiment. Data represent mean ± SEM. (**G**) Mouse naïve CD4⁺ lymphocytes were activated under Th1- or Th17-cell-polarizing conditions for three days and then treated overnight with the indicated drug. Expression of IFNγ and IL-17 was then assessed by flow cytometry. Data represent mean ± SEM of a triplicate experiment. (**H**) Daily I.P. treatment with heptelidic acid attenuated the course of EAE. Data were pooled from five mice per group and represent mean ± SEM for each time point. (**I**) Proposed model of immune modulation by DMF, which may exploit a physiologic negative feedback function of endogenous fumarate. *$P < 0.05$ and **$P < 0.01$ by one-way ANOVA with Tukey's multiple comparison (A); one-way ANOVA with Dunnett's multiple comparison (B, C, E–G); and Mann–Whitney *U* test (H).

Dimethyl fumarate targets GAPDH and aerobic glycolysis to modulate immunity

Michael D. Kornberg, Pavan Bhargava, Paul M. Kim, Vasanta Putluri, Adele M. Snowman, Nagireddy Putluri, Peter A. Calabresi and Solomon H. Snyder

published online March 29, 2018

www.sciencemag.org/cgi/content/full/science.aan4665/DC1

Supplementary Materials for

Dimethyl fumarate targets GAPDH and aerobic glycolysis to modulate immunity

Michael D. Kornberg, Pavan Bhargava, Paul M. Kim, Vasanta Putluri, Adele M. Snowman, Nagireddy Putluri, Peter A. Calabresi, Solomon H. Snyder*

*Corresponding author. Email: ssnyder@jhmi.edu

Published 29 March 2018 on *Science* First Release
DOI: 10.1126/science.aan4665

This PDF file includes:

Materials and Methods:

Reagents

Unless otherwise stated, all biochemical reagents were purchased from Sigma-Aldrich, all cell culture reagents from Gibco, and all cytokines from PeproTech. Recombinant human GAPDH was purchased from Abcam (catalog # ab82633). Dimethyl fumarate (DMF) and monomethyl fumarate (MMF) were from Aldrich, catalog # 242926 and 651419, respectively. For in vitro treatments, solutions of DMF and MMF were made fresh on the day of use by dissolving in DMSO to a concentration of 100 mM. For oral treatment of mice, DMF was prepared as described below. Heptelidic acid (Cayman Chemical, catalog # 14079) was dissolved in DMSO to a concentration of 2 mg/ml, aliquoted, and stored at -20°C until use. Lipopolysaccharide (LPS) from *Escherichia coli* O55:B5 (Sigma, catalog # L6529) was prepared in sterile PBS to a concentration of 1 mg/ml and stored at −20°C until use. All LPS treatments were performed at 1 μg/ml for 24 hours. Oligomycin (Calbiochem, catalog # 495455) was dissolved in ethanol at a concentration of 100 mM and stored at −20°C. Solutions of 2-deoxyglucose (2-DG, Sigma, catalog # D6134) were made fresh on the day of use by dissolving in PBS to a concentration of 500 mM. All materials for the Seahorse extracellular flux analyzer assays were purchased from Agilent Technologies (formerly Seahorse Bioscience). Mammalian expression constructs were made as previously described (*30*). The Δ2R1 RNA oligonucleotide described in (*27*) (sequence 5'-GGAUCCAUUUAUUUAUUUAUUUAAGCUUGG-3'), both with and without a 3' biotin label, was custom synthesized by Dharmacon.

Antibodies

Primary antibodies for immunoblot: rabbit polyclonal anti-phospho-p70 S6 Kinase (Thr421/Ser424) (Cell Signaling Technology, catalog # 9204, used at 1:1,000 dilution), mouse monoclonal anti-HIF-1α (clone H1α67, Novus Biologicals, catalog # NB100-105SS, used at 2 μg/ml), rabbit monoclonal anti-Histone H3 (clone D1H2, Cell Signaling Technology, catalog # 4499, used at 1:1000 dilution), rabbit polyclonal anti-iNOS (Santa Cruz Biotechnology, catalog # sc-651, used at 0.2 μg/ml), rabbit monoclonal anti-NF-κB p65 (clone D14E12, Cell Signaling Technology, catalog # 8242, used at 1:1,000 dilution), rat monoclonal anti-HA (clone 3F10, Roche, catalog # 11867423001, used at 0.2 μg/ml), rabbit polyclonal anti-β-tubulin (Cell Signaling Technology, catalog # 2146, used at 1:1,000 dilution), mouse monoclonal anti-β-actin HRP-conjugated (clone AC-15, Abcam, catalog # ab49900, used at 1:10,000 dilution), mouse monoclonal anti-arginase-1 (clone E-2, Santa Cruz Biotechnology, catalog # sc-271430, used at 0.4 μg/ml). *Lymphocyte polarization*: hamster anti-mouse CD3e (clone 145-2C11, BD Pharmingen, catalog # 553058), soluble hamster anti-mouse CD28 (clone 37.51, BD Pharmingen, catalog # 553294), anti-mouse IL-4 (clone 11B11, BioLegend, catalog # 504108), anti-mouse IFNγ (clone H22, BioLegend, catalog # 513206). *Flow cytometry, surface*: APC-conjugated rat anti-mouse CD4 (clone RM4-5, BioLegend, catalog # 100516), PerCP-eFluor 710-conjugated rat anti-mouse CD4 (clone RM4-5, eBioscience, catalog # 46-0042-82), PerCP-Cy5.5-conjugated rat anti-mouse CD25 (clone PC61, BioLegend, catalog # 102030), FITC-conjugated rat anti-mouse CD127 (clone A7R34, BioLegend, catalog # 135008). *Flow cytometry, intracellular*: PE-conjugated rat anti-FoxP3 (clone FJK-16s, eBioscience, catalog # 12-5773-82), PE-Cy7-conjugated mouse anti-Tbet (clone 4B10, BioLegend, catalog # 644824), APC-conjugated rat anti-IL-17 (clone eBio17B7, eBioscience, catalog # 17-7177-81), FITC-conjugated rat anti-mouse IFNγ (clone XMG1.2, BioLegend, catalog # 505806).

Animals

Wild-type C57BL/6J mice were purchased from The Jackson Laboratory and housed in a dedicated Johns Hopkins mouse facility. All protocols were approved by the Johns Hopkins Institutional Animal Care and Use Committee.

Treatment of mice with DMF

A suspension of 10 mg/ml DMF in 0.8% methyl cellulose (Sigma-Aldrich, catalog # 64632) solution was prepared and stored at 4°C when not in use for up to one week. Prior to each use, the suspension was allowed to warm to room temperature while stirring (at least 30 minutes). After bringing the suspension to the animal facility, the suspension was stirred again for a minimum of ten minutes prior to dosing.

Mice were treated daily for five consecutive days with 100 mg/kg DMF or vehicle control (0.8% methyl cellulose solution) by oral gavage. Two hours after the final dose, mice were sacrificed, and tissues were processed for GAPDH enzyme activity assay or GAPDH immunoprecipitation followed by mass spectrometric analysis, as described below.

Peripheral blood mononuclear cell (PBMC) isolation

Phlebotomy was performed on participants who provided informed consent under a protocol approved by the Johns Hopkins Institutional Review Board. Thirty milliliters of blood was obtained by venipuncture and immediately processed. PBMCs were separated using density gradient centrifugation with lymphocyte separation medium (LSM, MP Biomedicals). A standardized protocol was used as previously described (*31*). PBMCs were stored with a cryoprotectant in liquid nitrogen until use.

Preparation of samples for protein mass spectrometry

For mass spectrometric analysis of drug-treated recombinant GAPDH, 5 μg of recombinant protein was incubated with 50 μM DMF or 100 μM MMF in 50 μl of HEN buffer (250 mM Hepes-NaOH pH 7.7, 1 mM EDTA, 0.1 mM neocuproine) for 3 hours at 37°C. Samples were then stored at −70°C prior to analysis.

Mouse spleens and brains were homogenized in ice-cold RIPA buffer (50 mM Tris pH 7.4, 150 mM NaCL, 1% triton, 0.5% sodium deoxycholate, 0.1% SDS, 1 mM EDTA, protease inhibitors) using a Brinkmann POLYTRON™ homogenizer. Human PBMCs were lysed by sonication in ice-cold RIPA buffer. Lysates were cleared by centrifugation, and GAPDH was immunoprecipitated by incubating cleared lysates with rabbit monoclonal anti-GAPDH antibody (clone EPR1689, Abcam, ab181602, used at 18.5 μg/ml) overnight at 4°C. Protein A/G PLUS-Agarose beads (30 μl, Santa Cruz Biotechnology) were then added, and samples were incubated for an additional two hours at 4°C. The beads were then washed five times with RIPA buffer, aspirated to dryness with a 30-gauge needle, and resuspended/boiled in 30 μl SDS sample buffer. The samples were resolved by SDS–polyacrylamide gel electrophoresis (SDS–PAGE), and gel was stained with SimplyBlue™ SafeStain (Invitrogen). Gel bands containing GAPDH (discriminated based on size, approx. 37 kD) were excised and stored at −70°C until analysis.

Mouse samples were obtained from two DMF-treated and two vehicle-treated mice. Human samples were obtained from three DMF-treated MS patients, two MS patients not treated with DMF, and two healthy donor controls.

Liquid chromatography-tandem mass spectrometry (LC-MS/MS)

LC-MS/MS was performed by the Johns Hopkins University School of Medicine Mass Spectrometry and Proteomics Core Facility.

In–gel digestion of protein bands excised from gels was performed as previously described (*32*), with slight modifications. The proteins were reduced with dithiothreitol and alkylated with iodoacetamide in gel. The digestion buffer used was 10 mM triethylammonium bicarbonate. Peptides were injected onto a 2–cm trap column at 5 μl/minute for six minutes before being eluted onto a 75–μm 15–cm–long in–house packed column (Michrom Magic C18AQ, 5 μm 100 A) using an Easy-LC system (Thermo) operating at 300 nL/min. Each sample was run on a 60-minute gradient with double sawtooth cleanup gradients between each run. The peptides were eluted and ionized into a Q-Exactive plus mass spectrometer (Thermo Fisher) at 2.2 kV using a data-dependent ‘‘Top 15’’ method operating in FT–FT acquisition mode. The survey full-scan MS (m/z from 350–1800) was performed at a resolution 140,000 with an AGC target of 3e6, while the ion trap MS2 scans were performed at a resolution of 35,000 and a target AGC of 1×10^5 ions. Maximum injection times were set to 100 ms in the MS and 150 ms in the MS2. The ion selection intensity threshold was set to 3.3×10^4 counts and an isolation width of 1.9 Da, with a normalized collision energy of 27. Dynamic exclusion of 15 seconds was also used. Ambient polysiloxane produced a background peak at 371.101230 m/z, which was used as an internal calibrant for each survey scan.

LC-MS/MS protein data analysis

Tandem mass spectra were extracted by Proteome Discoverer version 1.4. Charge state deconvolution and deisotoping were performed using MS2 spectrum processor. All MS/MS samples were analyzed using Mascot (Matrix Science, London, UK; version 2.5.1). Mascot was set up to search the RefSeq2015_Complete database (downloaded 1/7/2015) assuming the digestion enzyme trypsin and one possible missed cleavage. Mascot was searched with a fragment ion mass tolerance of 0.030 Da and a parent ion tolerance of 12 PPM. Deamidated asparagine and glutamine, oxidation of methionine, carbamidomethyl of cysteine, 2-succinyl of cysteine, 2-monomethylsuccinyl of cysteine and 2-dimethylsuccinyl of cysteine were specified in Mascot as variable modifications.

Scaffold (version Scaffold_4.7.3, Proteome Software Inc., Portland, OR) was used to validate MS/MS based peptide and protein identifications. Peptide identifications were accepted if they could be established at greater than 95.0% probability by the Peptide Prophet algorithm (*33*) with Scaffold delta-mass correction. Protein identifications were accepted if they could be established at greater than 95.0% probability and contained at least 1 identified peptide. Protein probabilities were assigned by the Protein Prophet algorithm (*34*). Proteins that contained similar peptides and could not be differentiated based on MS/MS analysis alone were grouped to satisfy the principles of parsimony. GAPDH peptides with modification of the catalytic cysteine were inspected manually and accepted only if they were well fragmented with contiguous band y-ion stretches and showed complementary b- and y-ions.

Preparation of mouse peritoneal macrophages (mPMs)

Mice aged 8–12 weeks were each injected intraperitoneally with 2 ml of 3% sterile thioglycollate (BD Biosciences, catalog # 211716) medium. The mice were sacrificed 3–5 days later, and cells were harvested by peritoneal lavage with ice-cold RPMI medium containing 2% fetal bovine serum (FBS) and 1 unit/ml heparin. The cells were pelleted by centrifugation at $500 \times g$ for eight minutes, washed in ice-cold RPMI containing 2% FBS alone, pelleted by centrifugation, and re-suspended in ice-cold Spinner-modification minimum essential medium (SMEM, Sigma, M8167) supplemented with 10% FBS, 2 mM glutamine, and penicillin-streptomycin (SMEM-complete). Cells were then counted, and equal numbers were plated into each well of appropriate cell culture dishes. The cells were then incubated at 37°C for 2–4 hours to allow macrophage adhesion. Contaminating non-adherent cells

were then removed by washing culture dishes five times with ice-cold sterile PBS. Fresh SMEM-complete was then added to the plates, which were incubated overnight at 37°C prior to use in experiments. Additional treatments were performed in SMEM-complete medium unless otherwise specified.

Isolation of $CD4^+$ lymphocytes

Mouse naïve $CD4^+$ lymphocytes were isolated from the spleens of 7–11–week–old female C57BL/6J mice. Single-cell suspensions were generated in FACS buffer (PBS supplemented with 2% FBS and 1 mM EDTA) by disrupting spleens with the plunger of a syringe over a 70–μm nylon cell strainer (BD Falcon), pelleting cells by centrifugation (500 × *g* for eight minutes), and re-suspending in fresh FACS buffer. Naïve $CD4^+$ lymphocytes were then isolated by negative selection using an EasySep™ isolation kit (STEMCELL Technologies, catalog # 19765), according to manufacturer's protocol. For downstream applications, the cells were resuspended in mouse complete RPMI medium (mouse cRPMI, consisting of RPMI-1640 with GlutaMAX supplement plus 10% FBS, penicillin-streptomycin, glutamine supplement, 10 mM HEPES, 1 mM sodium pyruvate, 1x MEM NEAA, and 55 μM 2-mercaptoethanol).

For isolation of $CD4^+$ lymphocytes from human PBMCs, PBMCs were thawed and washed with human complete RPMI medium (human cRPMI, consisting of RPMI-1640 with GlutaMAX supplement plus 10% FBS, penicillin–streptomycin, and 50 μM 2-mercaptoethanol) and then re-suspended in FACS buffer. CD4+ lymphocytes were then isolated by negative selection using an EasySep™ isolation kit (STEMCELL Technologies, catalog # 17952), according to manufacturer's protocol.

GAPDH enzyme activity assays

Assays were performed in 10 mM sodium pyrophosphate buffer (pH 8.5) in 96-well plates. Recombinant GAPDH or cell/tissue lysates were incubated with 20 mM sodium arsenate (made fresh on day of experiment), 1 mM NAD^+, and 2.88 mM glyceraldehyde-3-phosphate (G3P). Enzyme activity was measured using a microplate–reader spectrophotometer (Molecular Devices) as the increase in absorbance at 340 nm due to reduction of NAD^+. The assay was performed at room temperature. The recombinant GAPDH or lysate was first diluted into sodium pyrophosphate buffer to a volume of 100 μl. An additional 100 μl of reaction mix containing the sodium arsenate, NAD^+, and G3P was then rapidly added to each well using a repeat pipettor, the plate was mixed for 5 seconds in the plate reader, and measurements then began. Absorbance was measured every 10–20 seconds for 20 minutes, and the rate was calculated from the change in absorbance during the linear phase.

For assays using recombinant GAPDH, 2 μg of enzyme was diluted to 500 μl (final concentration ~ 110 nM) in HEN buffer (250 mM Hepes-NaOH pH 7.7, 1 mM EDTA, 0.1 mM neocuproine) and treated with the indicated concentrations of DMF, MMF, or DMSO (as vehicle-treated control) at 37°C. At the indicated time points, aliquots were removed and subjected to the enzyme activity assay. In the experiment confirming that DMF inhibition of GAPDH is irreversible, recombinant GAPDH was treated as above with 100 μM DMF for 30 minutes, and the sample was then desalted twice with Zeba desalt spin columns (Thermo Scientific, catalog # 89882) to decrease the DMF concentration to less than 0.25 μM prior to enzyme assay. In the experiment examining whether active-site binding is required for DMF inhibition, recombinant GAPDH was pre-incubated with 500 μM G3P or NAD^+ for 15 minutes at room temperature prior to treatment with 50 μM DMF for 30 minutes at 37°C.

Cell and tissue lysates were prepared in GAPDH lysis buffer (20 mM Tris pH 7.8, 100 mM NaCL, 1% triton, protease inhibitors) either by passage through a 26-gauge needle (for cell lysates) or

homogenization with a Brinkmann POLYTRON™ homogenizer (mouse tissue), followed by centrifugation. Enzyme activity was measured from 0.5 μg of cell lysate and 2 μg of tissue lysate.

Determination of kinetics of GAPDH inactivation by DMF and MMF

The kinetic parameters K_i and k_{inact} were calculated from linear regression Kitz–Wilson plots as described (*20*), with the y-intercept equal to $\ln(2)/k_{inact}$, and the x-intercept equal to $-1/K_i$.

Lactate assay from mPMs

Lactate was measured by colorimetric assay from culture medium using the Glycolysis Cell–Based Assay Kit from Cayman Chemical (catalog # 600450). mPMs were harvested as described above and seeded into 24-well plates. After overnight culture, cells were washed with sterile PBS, and the media was replaced with serum-free SMEM supplemented with 2 mM glutamine and penicillin–streptomycin. Cells were then treated simultaneously with the indicated doses of DMF or MMF (or DMSO alone as vehicle control) in the presence or absence of 1 μg/ml LPS. After 24 hours, culture medium was collected, contaminating cellular debris was pelleted by centrifugation at 500 × *g* for eight minutes, and the supernatant was used for the assay as per manufacturer's instructions.

Seahorse extracellular flux analyzer assays for glycolysis

For experiments using mPMs, cells were harvested as described above and seeded directly into Seahorse XF96 cell culture microplates. After overnight culture, the medium was removed, cells were washed once with sterile PBS, and fresh SMEM-complete medium was added with/without 1 μg/ml LPS and the indicated concentrations of other drugs. After 18–24 hours at 37°C, medium was changed to glucose-free Seahorse XF assay medium containing 2 mM glutamine (pH adjusted to 7.4 and sterile-filtered), and cells were kept at 37°C in a CO_2-free incubator for an additional 45 minutes to one hour prior to the assay.

The protocol for lymphocyte assays was adapted from (*35*). Mouse naïve $CD4^+$ lymphocytes were resuspended in mouse cRPMI containing 3 μg/ml soluble anti-CD28 antibody and seeded at 1×10^6 cells/ml in 24-well plates pre-coated (overnight at 4°C) with 3 μg/ml anti-CD3 antibody. Cells were then treated with the indicated doses of DMF, MMF, or DMSO and cultured for 24 hours at 37°C prior to the assay. For experiments using human $CD4^+$ lymphocytes, cells suspended in human cRPMI were seeded at 1×10^6 cells/ml in 24-well plates and stimulated for 24–72 hours (as described in text/figures) with anti-CD3/anti-CD28 coated beads (Dynabeads, Life Technologies), with DMF or DMSO treatment during the final 24 hours of stimulation. On the day of the assay, cells were pelleted by centrifugation, washed once in XF assay medium (prepared as above), pelleted, and re-suspended in fresh XF assay medium. Cells were then counted, and equal numbers of viable cells (80–20 $\times 10^4$ per well) were plated onto a Seahorse XF96 cell culture microplate pre-coated with poly-D-lysine. After room-temperature centrifugation for 5 minutes at 400 × *g* to produce a uniform cell monolayer, additional XF assay medium was added to a final volume of 175 μl per well, and plates were kept at 37°C in a CO_2-free incubator for 30 minutes to one hour prior to the assay.

The extracellular acidification rate (ECAR) was measured using a Seahorse XFe96 Analyzer. Sensor cartridges (pre-hydrated in XF calibrant solution overnight in a CO_2-free incubator) were loaded with glucose (Port A), oligomycin (Port B), and 2-deoxyglucose (Port C) to achieve concentrations of 10 mM, 1 μM, and 50 mM, respectively, after injection. In experiments assessing the effect of oligomycin on DMF/MMF inhibition of glycolysis, oligomycin was included in the XF assay medium. Three measurements were obtained prior to each port injection, and after injection of Port C, with a

measurement loop of one-minute mix, two-minute wait, and three-minute measure. Data were analyzed using the XF Glycolysis Stress Test Report Generator.

Seahorse extracellular flux analyzer assays for oxidative phosphorylation (OXPHOS)

The assay was performed as described above for mPMs, except that the XF assay medium contained 2 mM glutamine, 1 mM sodium pyruvate, and 10 mM glucose. The sensor cartridge was loaded with oligomycin (Port A), FCCP (Port B), and rotenone/antimycin A (Port C) to achieve final concentrations of 1 μM, 1 μM, and 0.5 μM, respectively, after injection. As above, in experiments assessing the effect of oligomycin on DMF/MMF augmentation of OXPHOS, oligomycin was included in the XF assay medium. Oxygen consumption rate (OCR) was measured using the measurement protocol described above, and data was analyzed using the XF Mito Stress Test Report Generator.

Cell viability assays

Viability of mPMs was assessed by trypan blue exclusion. Cells were scraped from the culture plate, re-suspended in culture media by pipetting, and the cell suspension was diluted with 0.4% trypan blue stain (Invitrogen). Live/dead cells were counted manually under a light microscope using a hemocytometer.

For Seahorse assays, viability of lymphocytes was assessed either by trypan blue exclusion with manual counting using a hemocytometer (performed as above), or by propidium iodide staining followed by automated cell counting using a MACSQuant™ flow cytometer (Miltenyi Biotec). For assessment of viability in T–cell–polarization experiments, cells were stained with LIVE/DEAD aqua (Life Technologies, L-34966) as described below.

Glycolytic flux analysis with $U^{13}C$-glucose tracing

mPMs seeded into 10-cm plates were treated with 1 μg/ml LPS plus 25 μM DMF or DMSO in SMEM-complete medium. After six hours at 37°C, the cells were washed twice with glucose-free Dulbecco Modified Eagle Medium (DMEM) containing 10% FBS, 2 mM glutamine, and penicillin–streptomycin (glucose-free cDMEM). Fresh glucose-free cDMEM was then added, along with fresh LPS (1 μg/ml) and DMF (25 μM) or DMSO. After overnight glucose starvation, 12 mM $U^{13}C$-glucose (Cambridge Isotope Laboratories, catalog # CLM-1396) was added, and cells were incubated for six additional hours. The plates were then washed extensively with PBS and snap-frozen in liquid nitrogen. The frozen plates were then shipped on dry ice to the Baylor College of Medicine Metabolomics Core Facility for metabolite extraction and targeted mass spectrometry.

Isotope labeling by targeted mass spectrometry

Samples were prepared as described (*36–38*). Cells were scraped into a 500-μl mixture of 1:1 water/methanol, sonicated for one minute (two 30-second pulses), and then mixed with 450 μl of ice-cold chloroform. The resulting homogenate was then mixed with 150 μl of ice-cold water and vortexed again for two minutes. The homogenate was incubated at –20°C for 20 minutes and centrifuged at 4°C for ten minutes to partition the aqueous and organic layers. The aqueous and organic layers were combined and dried at 37°C for 45 minutes in an automatic Environmental Speed Vac system (Thermo Fisher Scientific). The extract was reconstituted in a 500-μl solution of ice-cold methanol/water (1:1) and filtered through a 3-kDa molecular filter (Amicon Ultracel 3-kDa Membrane) at 4°C for 90 minutes to remove proteins. The filtrate was dried at 37°C for 45 minutes in a speed vacuum and stored at –80°C until mass spectrometric analysis. Prior to mass spectrometric analysis, the dried extract was

resuspended in a 50-µl solution of methanol/water (1:1) containing 0.1% formic acid and then analyzed using multiple reaction monitoring (MRM). Ten microliters was injected and analyzed using a 6490 QQQ triple quadrupole mass spectrometer (Agilent Technologies) coupled to a 1290 Series HPLC system via selected reaction monitoring (SRM). Metabolites were targeted in both positive and negative ion modes: the electrospray source ionization (ESI) voltage was +4,000 V in positive ion mode and –3,500 V in negative ion mode. Approximately 9–12 data points were acquired per detected metabolite. To target the TCA flux, the samples were delivered to the mass spectrometer via normal-phase chromatography using a Luna Amino column (4 µm, 100A 2.1 × 150 mm).

Heat maps were generated using Morpheus software (The Broad Institute, https://software.broadinstitute.org/GENE-E/index.html)

Immunoblotting

With the exception of immunoblotting for nuclear NF-κB, cells were lysed by sonication in RIPA buffer supplemented with protease inhibitors. For nuclear NF-κB immunoblotting, nuclear fractions were prepared using a Nuclear/Cytosol Fractionation Kit (BioVision, catalog # K266-25). Protein concentrations were measured by Bradford assay (Bio-Rad). Lysates were mixed with SDS sample buffer, boiled, and resolved by SDS–PAGE. Bands were transferred to PVDF Immobilon P membranes (Millipore) using a wet transfer, blocked in TBS-T containing 5% milk, and probed overnight at 4°C with primary antibody in the manufacturer-recommended staining solution. HRP-conjugated secondary antibodies were from Jackson ImmunoResearch. Immunoblots were visualized using the SuperSignal West ECL system (Thermo Scientific) followed by film exposure. Quantification of digitally scanned immunoblots was performed by densitometry analysis using ImageJ software.

Measurement of cytokine production by enzyme-linked immunosorbent assay (ELISA)

Culture supernatants were collected and cytokine production was assayed using ELISA kits for IL-1β (catalog # 88-7013-22) and IL-6 (catalog # 88-7064-22) purchased from eBioscience, according to manufacturer's instructions. Plates were read at 450 nm on a microplate-reader spectrophotometer (Molecular Devices). For experiments in low– versus high–glucose conditions, mPMs were initially plated overnight in SMEM-complete medium. Cells were then washed twice with PBS, the medium was replaced with glucose-free cDMEM, and the indicated concentration of glucose was added. Cells were kept in this medium for 3 hours at 37°C prior to treatment with LPS, DMF, and/or DMSO (as vehicle control) for an additional 24 hours.

Macrophage alternative activation

mPMs seeded in six-well plates were treated for 24 hours with 20 ng/ml recombinant mouse IL-4 (PeproTech, catalog #214-14), plus 25 µM DMF or DMSO. The expression of arginase-1 was then assessed by immunoblot.

Transfection of peritoneal macrophages

Transfection was performed using jetPEI™-Macrophage DNA Transfection Reagent (Polyplus Transfection), with slight modification of manufacturer's protocol. mPMs were harvested as above and seeded into 24-well plates at a confluency of approximately 30%. Prior to transfection, the cells were cultured for three days in SMEM-complete medium plus 50 ng/ml of recombinant murine GM-CSF (PeproTech, catalog # 315-03) to induce expression of mannose receptors. GM-CSF was then included in the culture medium at this concentration in all subsequent steps. The cells were then transfected with 2 µg of DNA and 4 µl of jet-PEI™-Macrophage reagent per well, according to the manufacturer's

protocol. The complexes were removed after six hours, cells were washed once with SMEM-complete medium, and fresh SMEM-complete medium was then added. The following day, the cells were treated with 1 μg/ml LPS plus DMF or DMSO for an additional 24 hours prior to cytokine ELISA assay.

DNA plasmids were prepared using an EndoFree Plasmid Maxi Kit (Qiagen) to eliminate contamination with endotoxins.

Polarization of mouse naïve $CD4^+$ lymphocytes

Mouse naïve $CD4^+$ lymphocytes isolated by negative selection (as described above) were suspended in mouse cRPMI and seeded into 96-well plates (200,000 cells per well) that had been coated overnight with anti-CD3 antibody. Polarization conditions were as follows: Th1 (3 μg/ml anti-CD3/CD28 antibodies, 5 ng/ml recombinant mouse IL-2, 10 ng/ml recombinant mouse IL-12, 5 μg/ml anti-IL-4 antibody); Th17 (5 μg/ml anti-CD3/CD28 antibodies, 20 ng/ml recombinant mouse IL-6, 5 ng/ml recombinant human TGF-β1, 10 ng/ml recombinant mouse IL-23, 10 ng/ml recombinant mouse IL-1β, 5 μg/ml anti-IL-4 antibody, 5 μg/ml anti-IFNγ antibody); and Treg (3 μg/ml anti-CD3/CD28 antibodies, 15 ng/ml recombinant human TGF-β1, 5 ng/ml recombinant mouse IL-2, 5 μg/ml anti-IL-4 antibody, 5 μg/ml anti-IFNγ antibody). The cells were cultured under these polarizing conditions for four days at 37°C prior to flow cytometric analysis. Cells were treated with the indicated doses of DMF, MMF, or heptelidic acid either at the onset of culture (day 0) or on day 3.

Flow cytometry and staining

On the morning of analysis, cells were pelleted by centrifugation and resuspended in fresh mouse cRPMI containing cell stimulation cocktail with protein transport inhibitors (eBioscience, catalog # 00-4975-03). The cells were incubated at 37°C for an additional 4–5 hours prior to staining. All staining procedures were performed in the dark at room temperature. To assess viability, cells were first stained with LIVE/DEAD aqua (Life Technologies, L-34966) for 30 minutes in PBS. The cells were then washed and stained with specific conjugated antibodies for surface markers in FACS buffer (PBS supplemented with 2% fetal bovine serum and 1mM EDTA) for 30 minutes. For intracellular staining of cytokines and transcription factors, cells were then permeabilized and fixed using FoxP3 fixation/permeabilization buffer (eBioscience, 00-5521-00) following the manufacturer–recommended protocol and incubated with specific conjugated antibodies for the specified proteins in permeabilization buffer for 45 minutes.

Cells were analyzed by flow cytometry using a MACSQuant™ flow cytometer (Miltenyi Biotec). A minimum of 50,000 cells were analyzed per sample with the exception of 25 μM DMF treatment under Th1– and Th17–cell–polarizing conditions, in which toxicity limited the number of cells that could be counted. Data analysis was performed in FlowJo (FlowJo, LLC).

RNA electrophoretic mobility shift assay (REMSA) for GAPDH–RNA binding

REMSA was performed using the LightShift Chemiluminescent RNA EMSA Kit from Thermo Scientific (catalog # 20158), according to manufacturer's instructions. The sequence for Δ2R1 was derived from (*27*).

Recombinant GAPDH (2 μg) was diluted in 50 μl HEN buffer. The indicated concentrations of DMF, heptelidic acid, or DMSO (as vehicle control) were then added, and the samples were incubated at 37°C for 30 minutes. Two microliters of the above solution was then included in a 20–μl GAPDH–

RNA binding reaction, which included 10 nM biotinylated Δ2R1 RNA oligonucleotide, 5% glycerol, and 2 μg tRNA (to block non-specific binding) in 1 x REMSA binding buffer. In the indicated samples, 200-fold molar excess (2 μM) of non-biotinylated Δ2R1 or NAD^+ was added to the binding reaction prior to addition of biotinylated Δ2R1. Binding was allowed to occur for 25 minutes at room temperature. Binding was stopped with the addition of REMSA loading buffer, and the sample was loaded into a 6% DNA retardation gel (Invitrogen, catalog # EC6465BOX) and electrophoresed in 0.5 x TBE buffer (45 mM Tris, 4 mM boric acid, 1 mM EDTA). Unbound RNA and GAPDH–RNA complexes were then transferred to PVDF membrane and UV crosslinked. Biotinylated Δ2R1 was detected by chemiluminescence, according to kit instructions.

Experimental autoimmune encephalomyelitis (EAE)

MOG_{35-55} peptide (amino acid sequence MEVGWYRSPFSRVVHLYRNGK) was prepared by the Johns Hopkins Synthesis and Sequencing Core Facility. Incomplete Freund's adjuvant was purchased from ThermoScientific (catalog # 77145), and complete Freund's adjuvant was prepared by adding 8 mg/ml of heat–killed *Mycobacterium tuberculosis* H37 Ra (Difco, catalog # 231141). Pertussis toxin was purchased from List Biologicals (catalog # 181).

Active EAE was induced in 8–12 week-old female C57BL/6J mice that had been allowed to acclimatize to the animal facility for at least one week. MOG_{35-55} peptide dissolved in PBS at a concentration of 2 mg/ml was mixed 1:1 with complete Freund's adjuvant to make an emulsion. On day 0, mice were immunized by injecting 50 μl of the emulsion subcutaneously into each of two sites on the lateral abdomen. In addition, on day 0 and again on day 2, mice were injected I.P. with 250 ng of pertussis toxin dissolved in PBS. Mice were weighed and scored beginning on day 7 post–immunization. Scoring was performed according to the following scale: 0 = no clinical deficit; 0.5 = partial loss of tail tone; 1.0 = complete tail paralysis or both partial loss of tail tone plus awkward gait; 1.5 = complete tail paralysis and awkward gait; 2.0 = tail paralysis with hind limb weakness evidenced by foot dropping between bars of cage lid while walking; 2.5 = hind limb paralysis with little to no weight-bearing on hind limbs (dragging) but with some movement possible in legs; 3.0 = complete hind limb paralysis with no movement in lower limbs; 3.5 = hind limb paralysis with some weakness in forelimbs; 4.0 = complete tetraplegia but with some movement of head; 4.5 = moribund; 5.0 = dead.

Heptelidic acid (2 mg/ml in DMSO) was diluted 1:9 in sterile PBS (for a final concentration of 0.2 mg/ml in 10% DMSO in PBS). Mice were then treated daily with 1 mg/kg heptelidic acid or an equal volume of vehicle control (10% DMSO in PBS) by intra-peritoneal injection beginning on day 5 post-immunization.

Statistical analysis

Statistical analysis was performed using Excel or Prism software. For comparisons of two groups, two-tailed Student's *t* test was performed. For comparisons of three or more groups, one-way ANOVA was performed with post-hoc multiple comparison testing using Tukey's (for comparison of each group to every other group) or Dunnett's (for comparison of each group to the control group) method. The results of EAE were analyzed by Mann-Whitney U-test.

Recombinant human GAPDH treated with MMF or DMF				
Charge: 2+	Expected mass (daltons)	Observed mass (daltons)		
		Vehicle	MMF	DMF
IISNAS**C(2MSC)**TTNC(Carb)LAPLAK	1905.917	-	1905.918	1905.92
IISNAS**C(2DSC)**TTNC(Carb)LAPLAK	1919.933	-	-	1919.933
Mice treated orally with dimethyl fumarate (100 mg/kg daily for 5 days)				
	Expected mass (daltons)	Observed mass (daltons)		
		Vehicle spleen	DMF spleen	DMF brain
IVSNAS**C(2MSC)**TTNC(Carb)LAPLAK	1891.902	-	1891.900	1891.903
IVSNAS**C(2DSC)**TTNC(Carb)LAPLAK	1905.918	-	1905.929	1905.918
PBMCs from patients treated with oral dimethyl fumarate for 3 months				
	Expected mass (daltons)	Observed mass (daltons)		
		MS control	DMF treated	
IISNAS**C(2MSC)**TTNC(Carb)LAPLAK	1905.917	-	1905.917	

Table S1. Observed and expected mass of peptides identified by LC-MS/MS to include succination of the active-site cysteine of GAPDH by either monomethyl (2MSC, +130 Da) or dimethyl (2DSC, +144 Da) fumarate. Because samples were reduced and treated with iodoacetate, non-succinated cysteines were modified with carbamidomethyl (Carb, +57 Da). The active-site cysteine and its associated modification are shown in bold. Recombinant GAPDH was treated with DMF (50 μM) or MMF (100 μM) for 3 hours at 37°C. For mouse and human experiments, GAPDH was immunoprecipitated from lysates and separated by protein electrophoresis prior to sending for mass spectrometric analysis. Data from recombinant GAPDH were analyzed from two pooled samples each of vehicle–, MMF–, and DMF–treated protein. Data from mice were analyzed from two pooled samples each of vehicle– and DMF–treated animals. Data from MS patients were analyzed from pooled samples of three DMF–treated and two non–DMF–treated patients. Da = daltons.

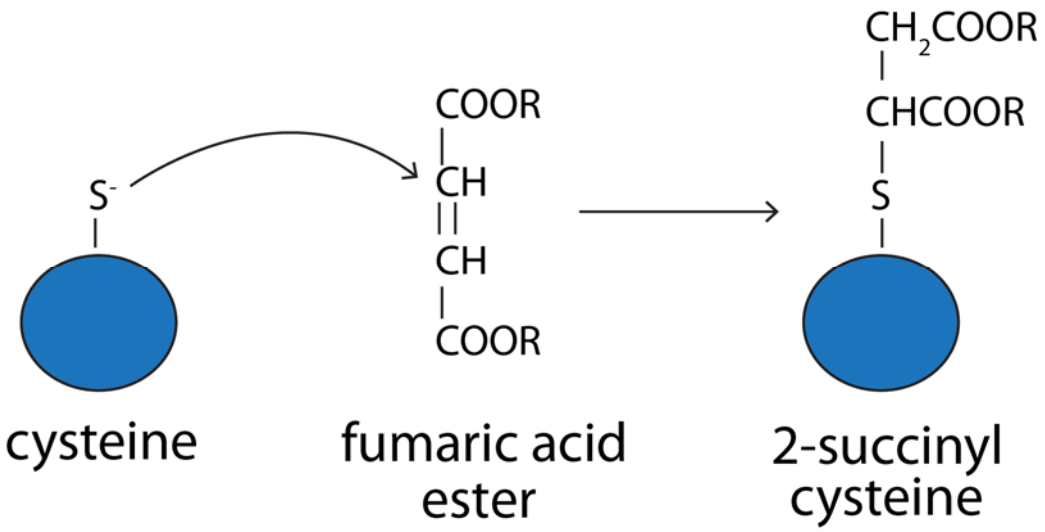

fig. S1. Succination by fumaric acid esters. Schematic diagram of the covalent, irreversible modification of cysteine residues by fumarate and its derivatives, termed succination.

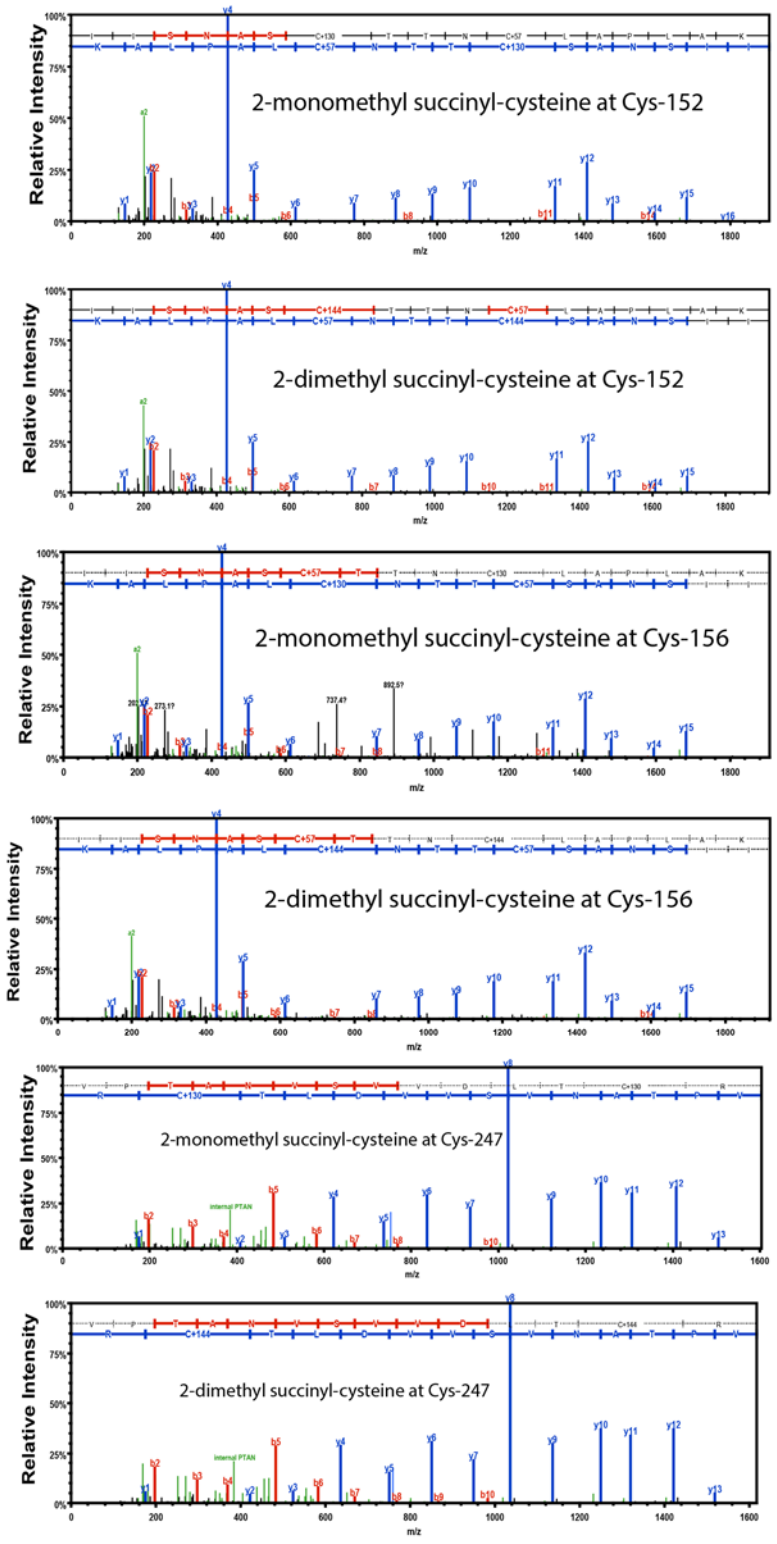

fig. S2. LC-MS/MS analysis of DMF– and MMF–mediated succination of recombinant GAPDH in vitro. Representative LC-MS/MS spectra demonstrating modification of GAPDH cysteines by either monomethyl (2-monomethyl succinyl-cysteine, +130 Da) or dimethyl (2-dimethyl succinyl-cysteine, +144 Da) fumarate in recombinant human GAPDH treated with DMF (50 μM) or MMF (100 μM) for 3 hours at 37°C. Data were analyzed from two pooled samples each of vehicle–, MMF–, and DMF–treated protein. Da = daltons.

A

GAPDH purified from vehicle-treated mouse spleen		
Charge: 2+	Expected mass (daltons)	Observed mass (daltons)
IVSNAS**C(2SC)**TTNC(Carb)LAPLAK	1877.872	1877.890
GAPDH purified from healthy control PBMCs		
Charge: 2+	Expected mass (daltons)	Observed mass (daltons)
IISN(De)AS**C(2SC)**TTNC(Carb)LAPLAK	1892.887	1892.900

B

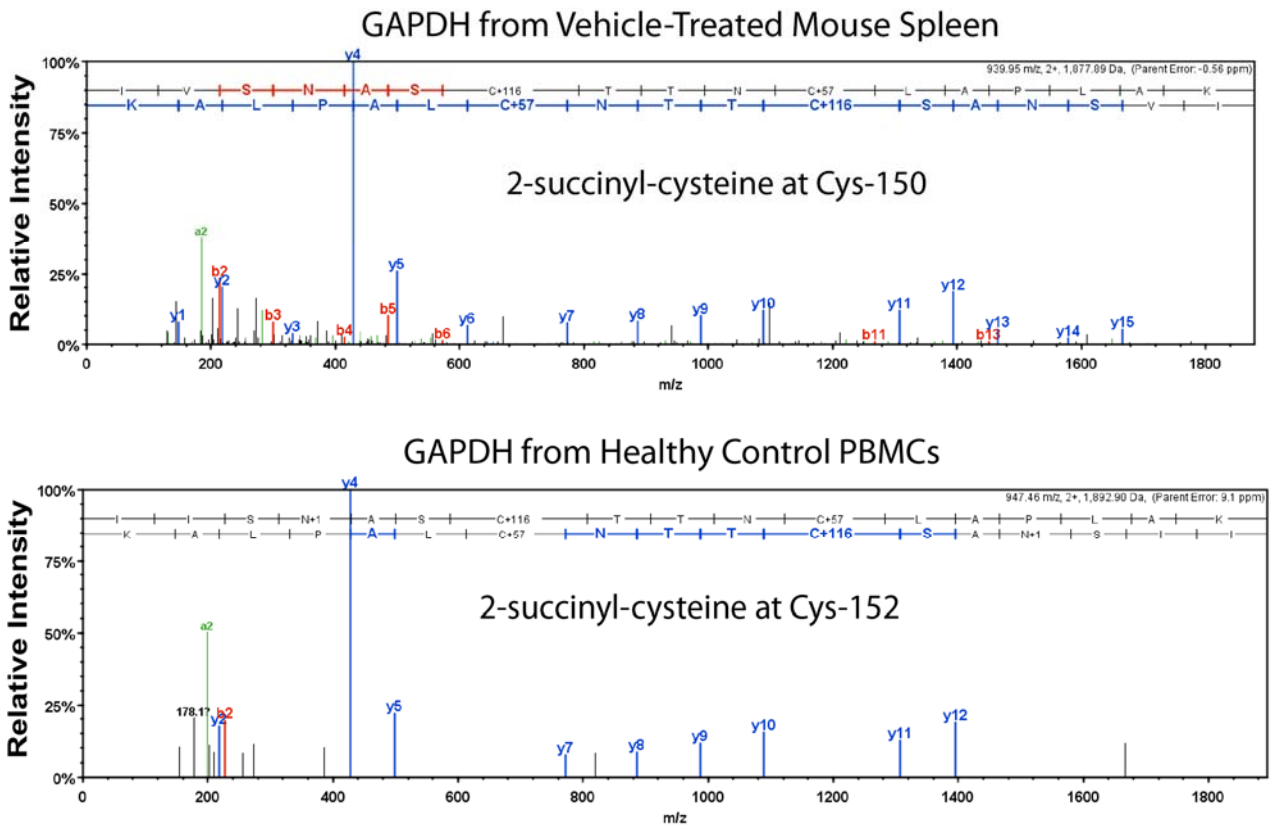

fig. S3. Succination of GAPDH active-site cysteine by endogenous fumarate in vivo. Mass table **(A)** and representative LC-MS/MS spectra **(B)** demonstrating 2-succinyl-cysteine (2SC, +116 Da) formation at the catalytic cysteine of GAPDH derived from vehicle-treated mice and healthy control PBMCs. Pooled samples were analyzed from two mice and two healthy controls. Da = daltons, De = deamidated, Carb = carbamidomethylated.

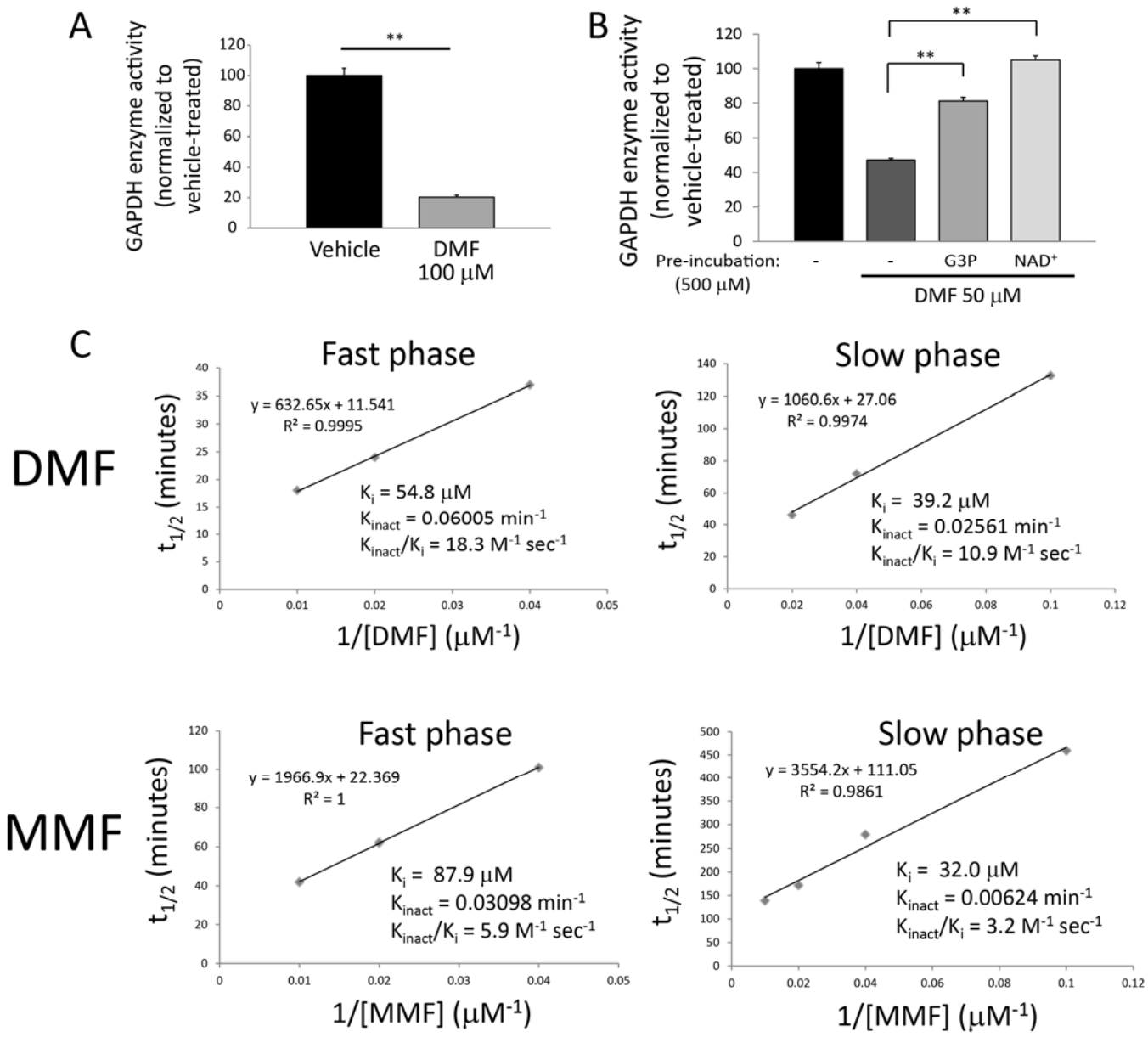

fig. S4. Kinetics of irreversible GAPDH inhibition by DMF and MMF. (A) Recombinant GAPDH was treated with 100 μM DMF or vehicle for 30 minutes, desalted twice to remove ≥ 99.75% of DMF (final concentration less than 0.25 μM), and then subjected to enzyme activity assay. Removal of DMF failed to restore GAPDH activity, indicating irreversible inhibition. Data represent mean ± SEM of a triplicate experiment. **(B)** Recombinant GAPDH was pre-incubated with or without 500 μM G3P or NAD^+, then treated with 50 μM DMF for 30 minutes prior to enzyme assay. Data represent mean ± SEM of a triplicate experiment. **(C)** Kitz–Wilson plots and associated DMF– and MMF–GAPDH inhibition kinetics derived from four experiments performed in duplicate. $^{**}P < 0.01$ by two-tailed Student's *t* test (A) and one-way ANOVA with Dunnett's multiple comparison (B).

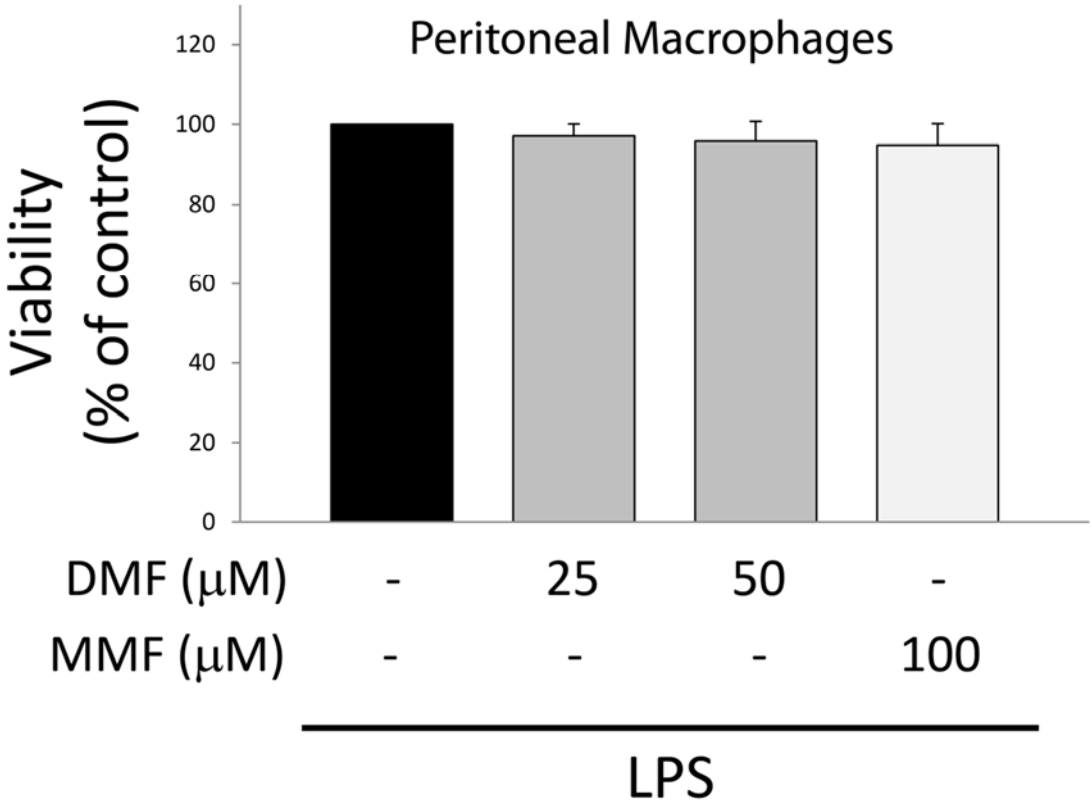

fig. S5. DMF and MMF have no effect on viability of LPS-stimulated macrophages. Mouse peritoneal macrophages were treated with 1 μg/ml LPS plus the indicated doses of DMF or MMF for 24 hours, and viability was assessed by trypan blue exclusion. Data represent mean ± SEM of four experiments performed in duplicate. Results are non-significant by one-way ANOVA.

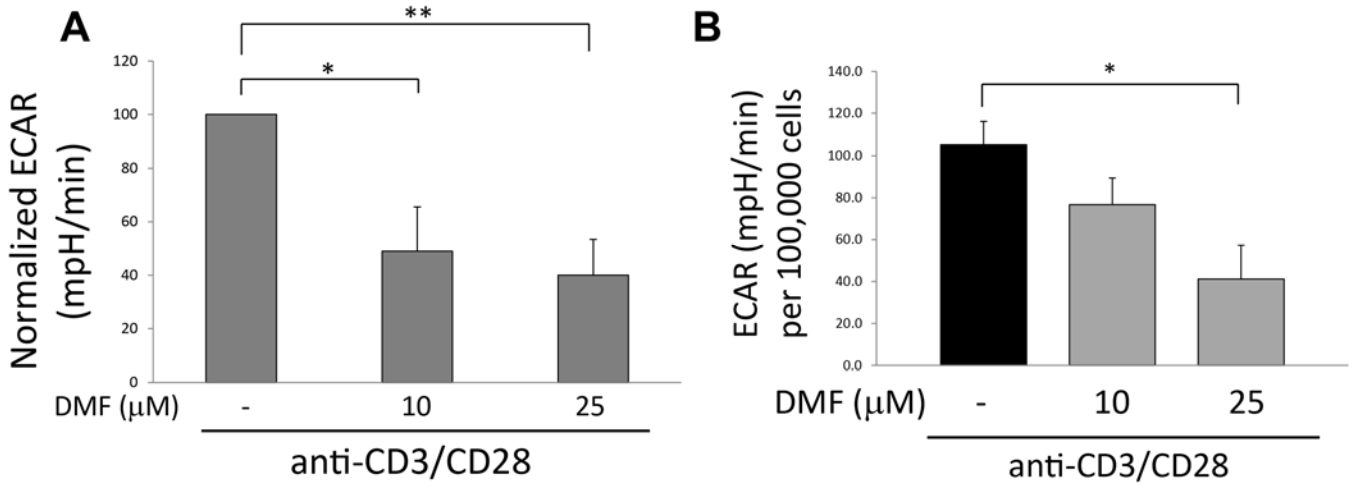

fig. S6. DMF inhibits aerobic glycolysis in activated human CD4$^+$ lymphocytes. (A) Glycolysis, measured as ECAR using a Seahorse extracellular flux analyzer, in human CD4$^+$ lymphocytes from healthy donors stimulated with 1 μg/ml each of anti-CD3/CD28 antibodies for 24 hours ± simultaneous treatment with DMF. Data represent mean ± SEM of four subjects, with assays performed in triplicate. **(B)** Experiment performed as in (A), except that cells were stimulated with anti-CD3/CD28 antibodies for 72 hours, with DMF treatment only during the final 24 hours of stimulation. Data represent mean ± SEM of three subjects, with assays performed in triplicate. *$P < 0.05$ and **$P < 0.01$ by one-way ANOVA with Dunnett's multiple comparison.

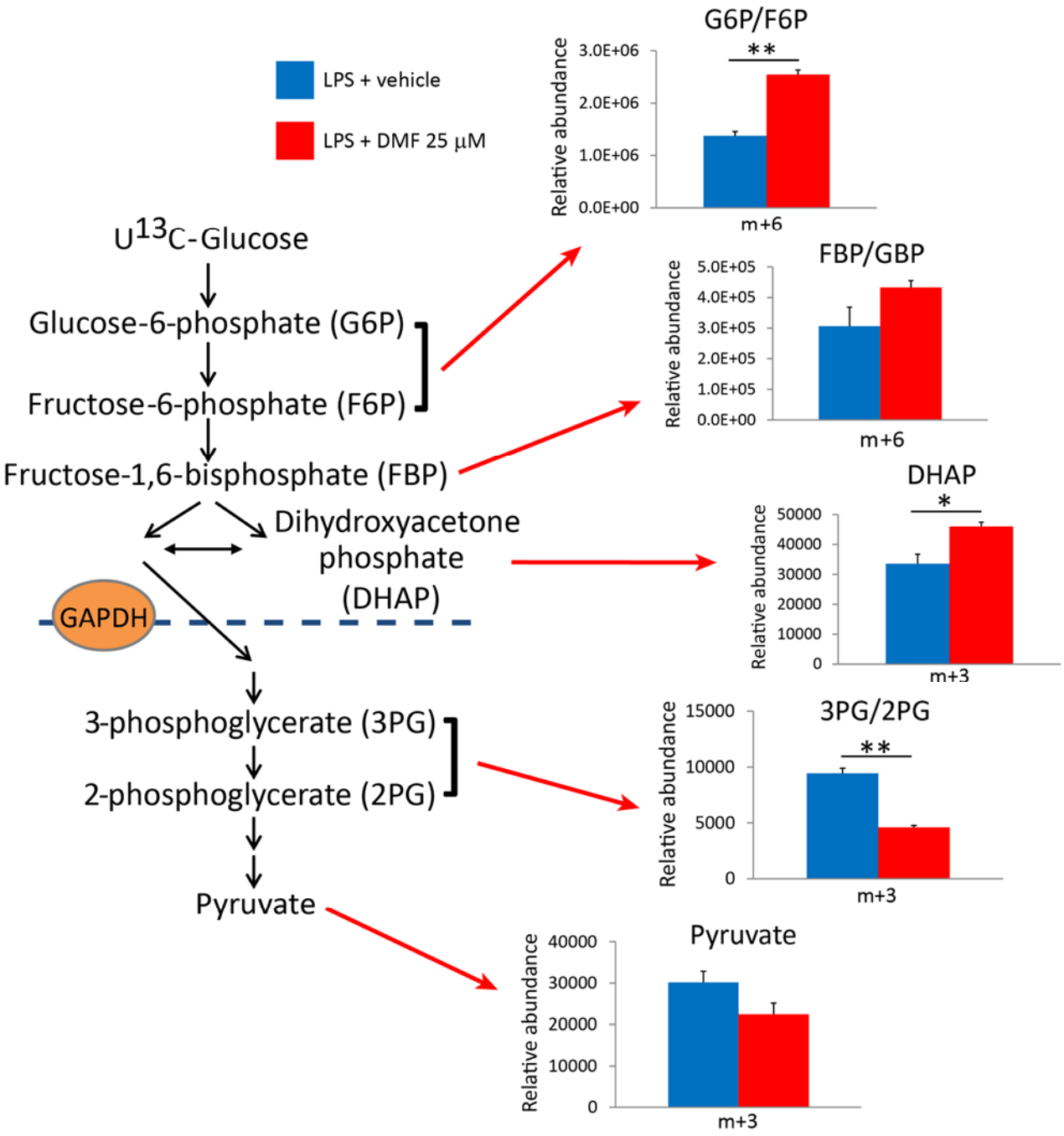

fig. S7. Effect of DMF on glycolytic flux in LPS-stimulated macrophages. Bar graphs (corresponding to heat map shown in Fig. 2D) showing the relative abundance of $U^{13}C$-labeled glycolytic intermediates in peritoneal macrophages stimulated with LPS for 24 hours ± 25 μM DMF, followed by labeling with $U^{13}C$-glucose. Data represent mean ± SEM of a triplicate experiment. *$P < 0.05$ and **$P < 0.01$ by two-tailed Student's *t* test.

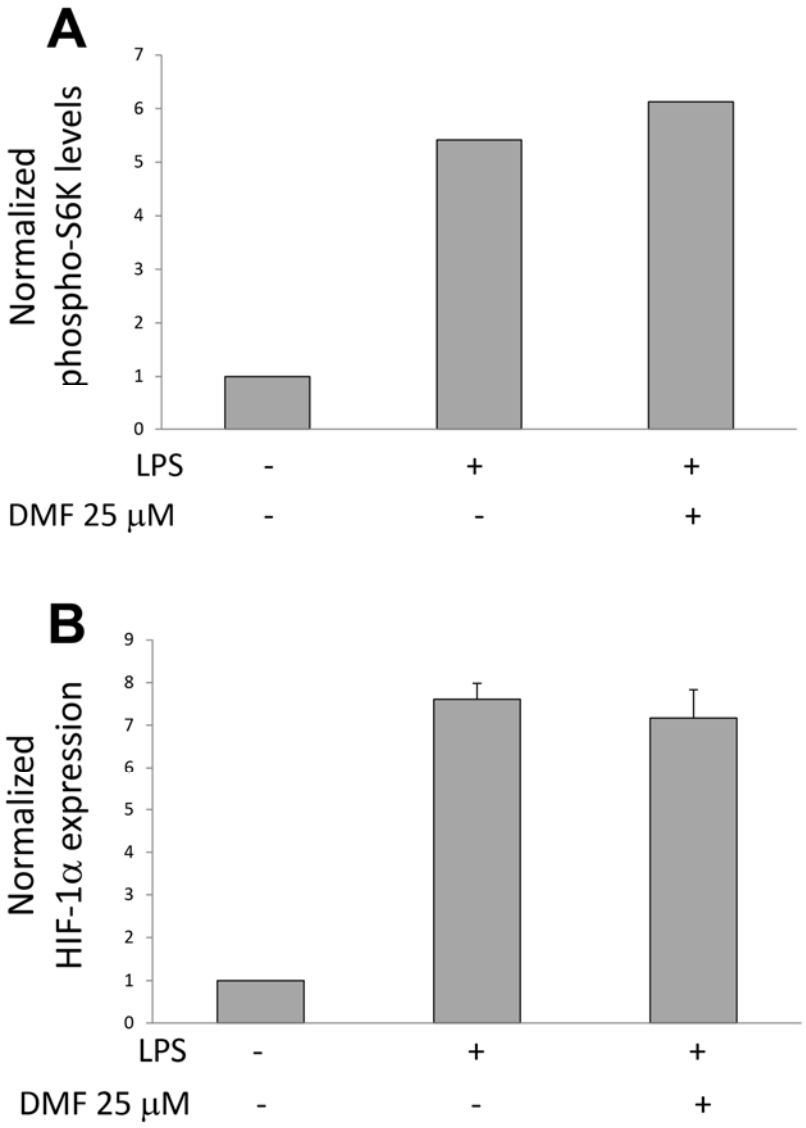

fig. S8. Quantification of phospho-S6K and HIF-1α levels after DMF treatment in mPMs. (**A**) Quantification of immunoblots for phospho-S6K in mPMs treated with 1 μg/ml LPS ± DMF for 24 hours. Data represent the mean of two experiments performed in duplicate and were corrected based on actin loading control. (**B**) Quantification of immunoblots for HIF-1α in mPMs treated as in (A). Data represent mean ± SEM of three experiments and were corrected based on histone H3 loading control.

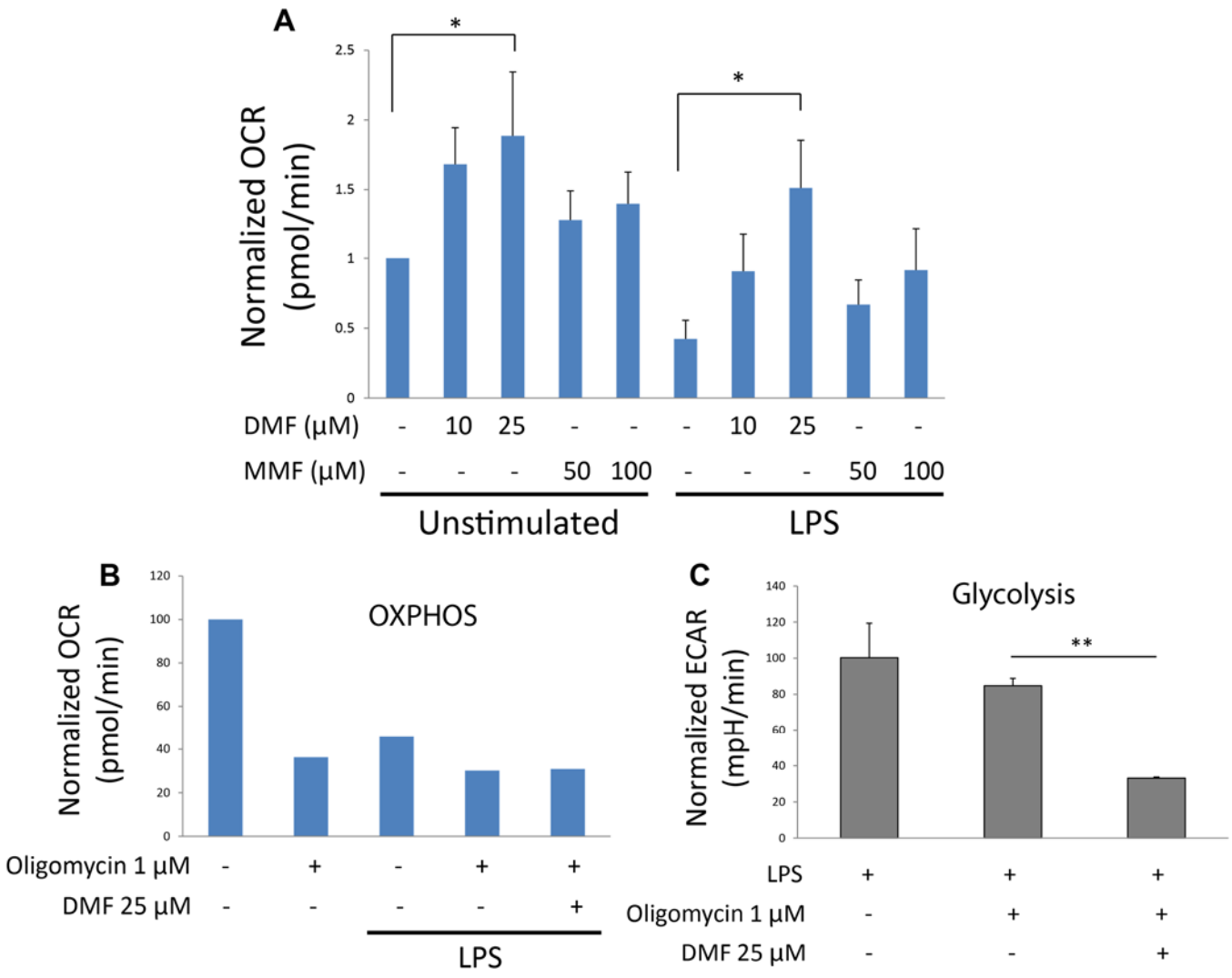

fig. S9. DMF and MMF augment oxidative phosphorylation in macrophages, but inhibition of glycolysis is independent of this effect. (**A**) Oxidative phosphorylation (OXPHOS), measured as oxygen consumption rate (OCR) using a Seahorse extracellular flux analyzer, in mPMs treated ± 1 μg/ml LPS and the indicated doses of drug. Data represent mean ± SEM of five experiments performed in quadruplicate. (**B**) Blocking mitochondrial respiration with oligomycin abolished the effect of DMF on OXPHOS. mPMs were treated with the indicated combinations of LPS, DMF, and oligomycin for 24 hours, followed by Seahorse assay. Seahorse assay was also conducted in the presence of oligomycin. Data represent the mean of two experiments performed in quadruplicate. (**C**) ECAR measured from LPS–stimulated mPMs ± DMF and oligomycin shows that DMF inhibited aerobic glycolysis even when its effects on OXPHOS were blocked with oligomycin. Cells were treated as in (B). Data represent mean ± SEM of three experiments performed in quadruplicate. **P* < 0.05 and ***P* < 0.01 by one-way ANOVA with Dunnett's (A) and Tukey's (C) multiple comparison.

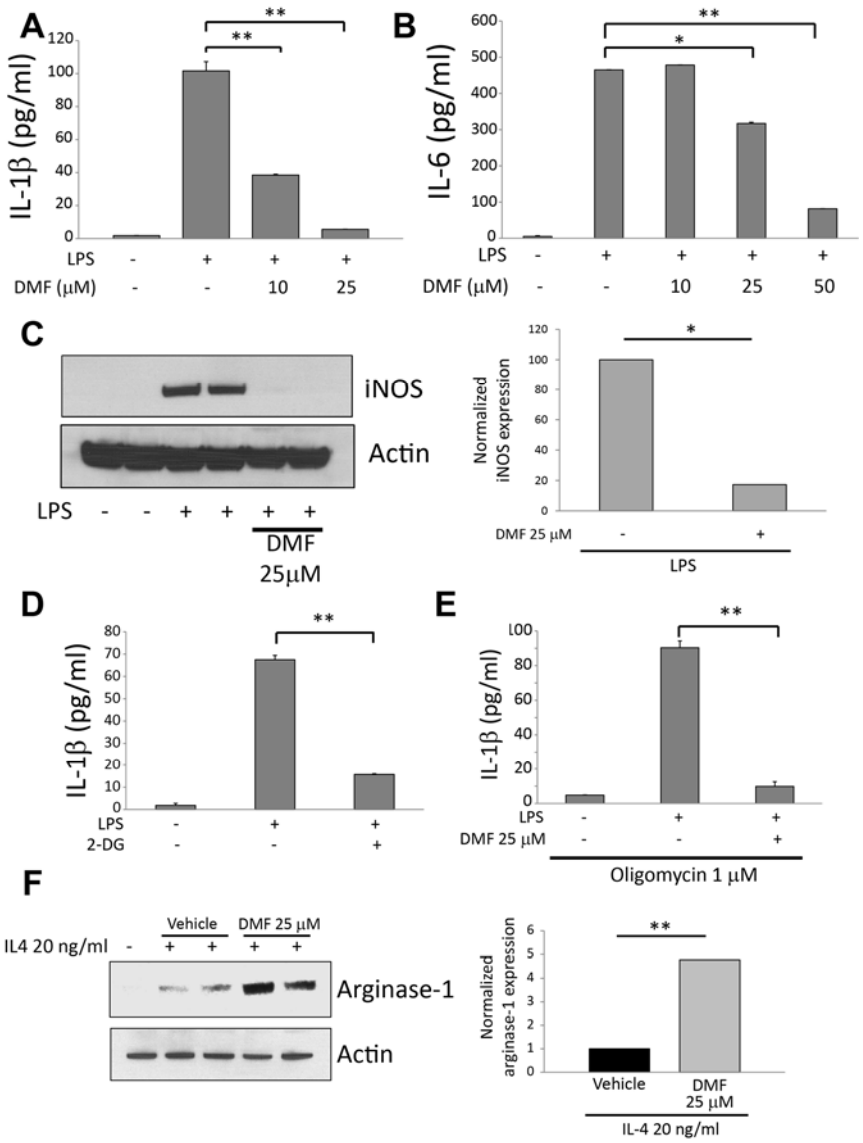

fig. S10. Effects of DMF and 2-deoxyglucose on classical and alternative macrophage activation. (**A** and **B**) ELISA assays from mPM culture media showing that DMF blocked secretion of the inflammatory cytokines IL-1β (A) and IL-6 (B). Data represent mean ± SEM of triplicate experiments. (**C**) (Left) Representative immunoblot from mPM lysates showing that DMF blocked LPS-induced expression of iNOS. (Right) Quantification of iNOS immunoblots. Data represent the mean of two experiments performed in duplicate and were corrected based on actin loading control. **(D)** mPMs were pre-treated for 3 hours with or without 5 mM 2-deoxyglucose (2-DG) in media containing 10 mM glucose and then stimulated with 1 μg/ml LPS for 24 hours. IL-1β was measured from culture media by ELISA. Data represent mean ± SEM of a triplicate experiment. **(E)** DMF inhibited IL-1β secretion in LPS-stimulated mPMs even when OXPHOS was blocked by oligomycin. Cells were treated ± 1 μg/ml LPS and the indicated doses of DMF and oligomycin for 24 hours, followed by IL-1β measurement from culture media via ELISA. Data represent mean ± SEM of a triplicate experiment. **(F)** (Left) Representative immunoblot of arginase-1 in mPMs treated with 20 ng/ml IL-4 for 24 hours ± 25 μM DMF. (Right) Quantification of arginase-1 immunoblots. Data represent the mean of two experiments performed in duplicate and were corrected based on actin loading control. **P* < 0.05 and ***P* < 0.01 by one-way ANOVA with Dunnett's multiple comparison (A–B) and two-tailed Student's *t* test (C–F).

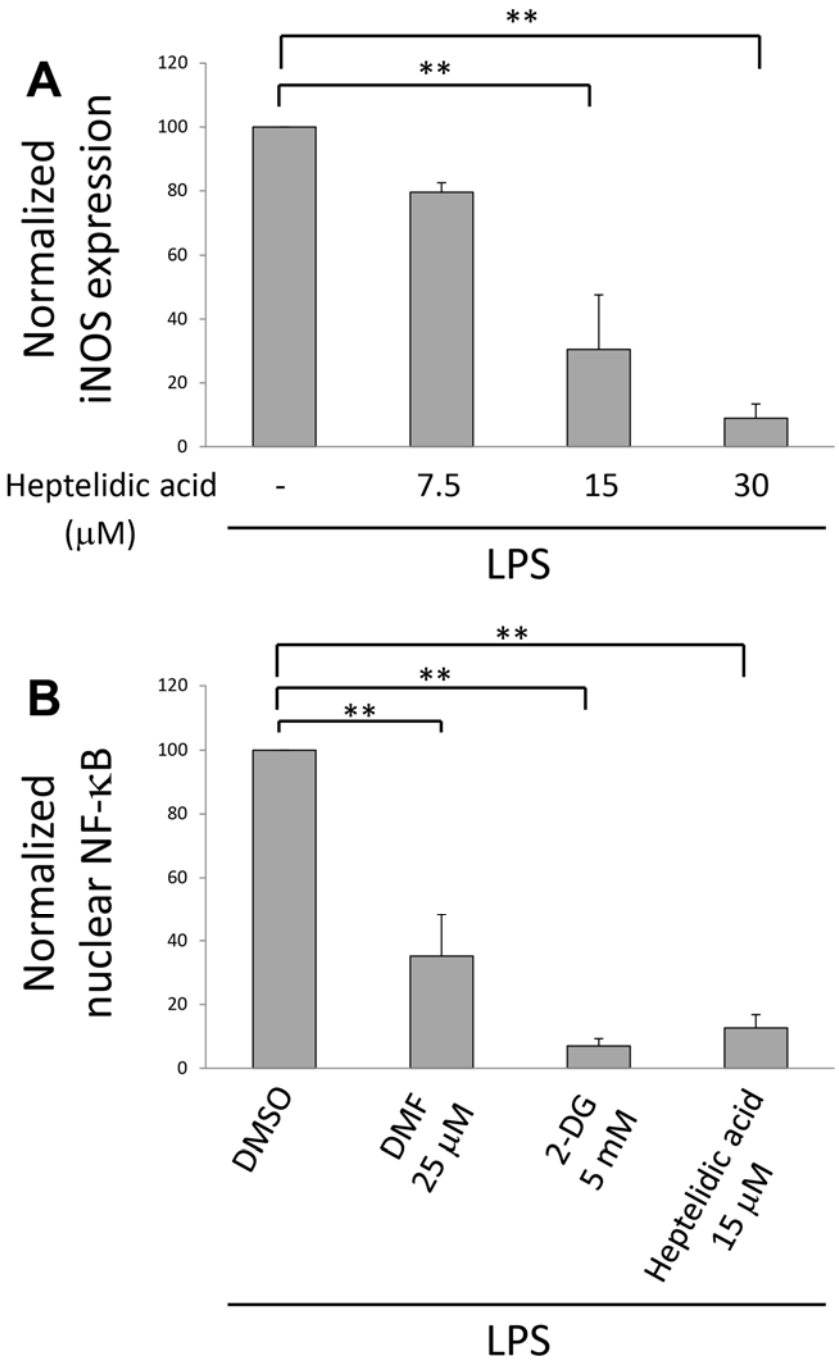

fig. S11. Quantification of iNOS and nuclear NF-κB immunoblot data depicted in Figure 3. (**A**) Quantification of immunoblots for iNOS in LPS-stimulated mPMs treated with the indicated doses of heptelidic acid. Data represent the mean ± SEM of three experiments and were corrected based on actin loading control. (**B**) Quantification of immunoblots for nuclear NF-κB in LPS-stimulated mPMs treated with the indicated drugs. Data represent the mean ± SEM of three experiments and were corrected based on histone H3 loading control. ***P* < 0.01 by one-way ANOVA with Dunnett's multiple comparison.

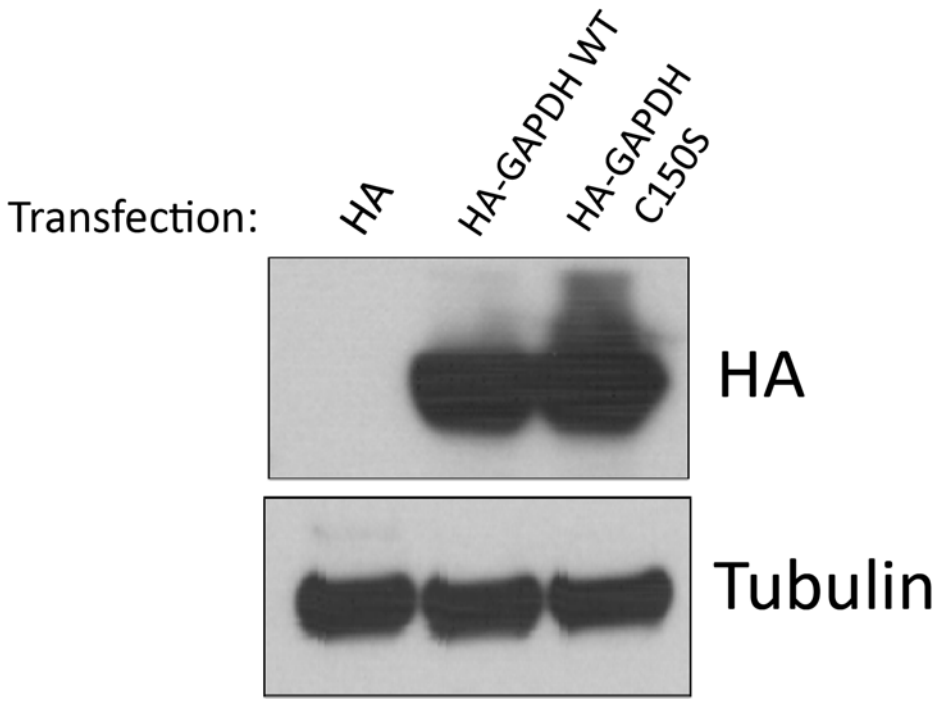

fig. S12. Successful transfection of mPMs with GAPDH constructs. mPMs were transfected as described in Methods with plasmids expressing HA-tagged empty vector, wild-type GAPDH (HA-GAPDH WT), or GAPDH Cys-150 mutant (HA-GAPDH C150S). Representative immunoblot from 20 μg lysate probed with anti-HA antibody shows successful overexpression of GAPDH constructs.

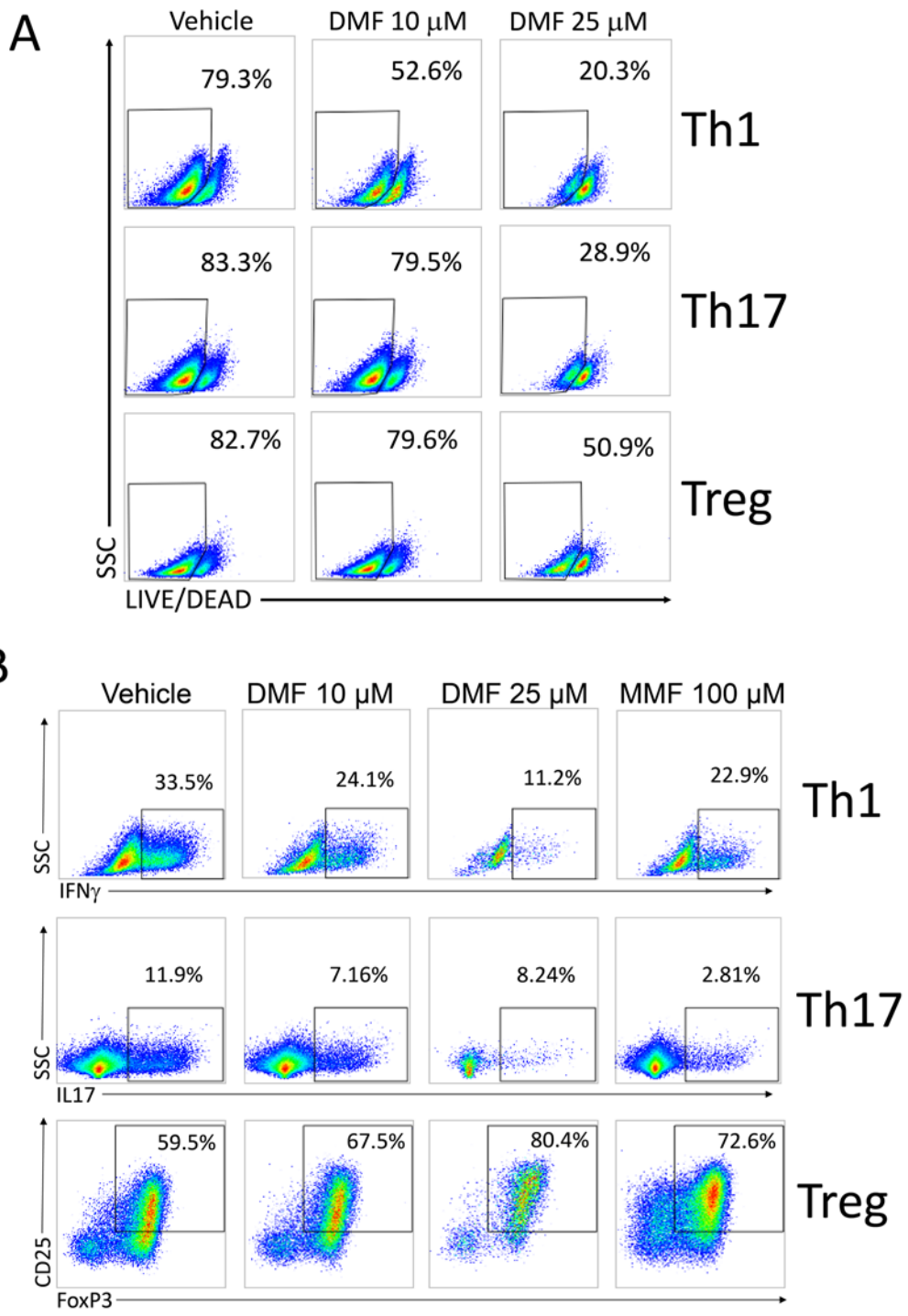

fig. S13. Representative flow cytometric plots from mouse naïve CD4⁺ lymphocytes activated for four days under polarizing conditions in the presence of DMF/MMF. Cells were activated with anti-CD3/CD28 antibodies under Th1–, Th17–, or Treg–cell–polarizing conditions for four days, with DMF treatment on day 0. Flow cytometry analysis was performed on day 4. **(A)** Flow cytometric plots representing data tabulated in Fig. 4A. Viability was assessed by LIVE/DEAD staining. **(B)** Flow cytometric plots representing data tabulated in Fig. 4, B, C, and E. IFNγ, IL17, and FoxP3 expression were assessed under Th1–, Th17–, and Treg–cell–polarizing conditions, respectively.

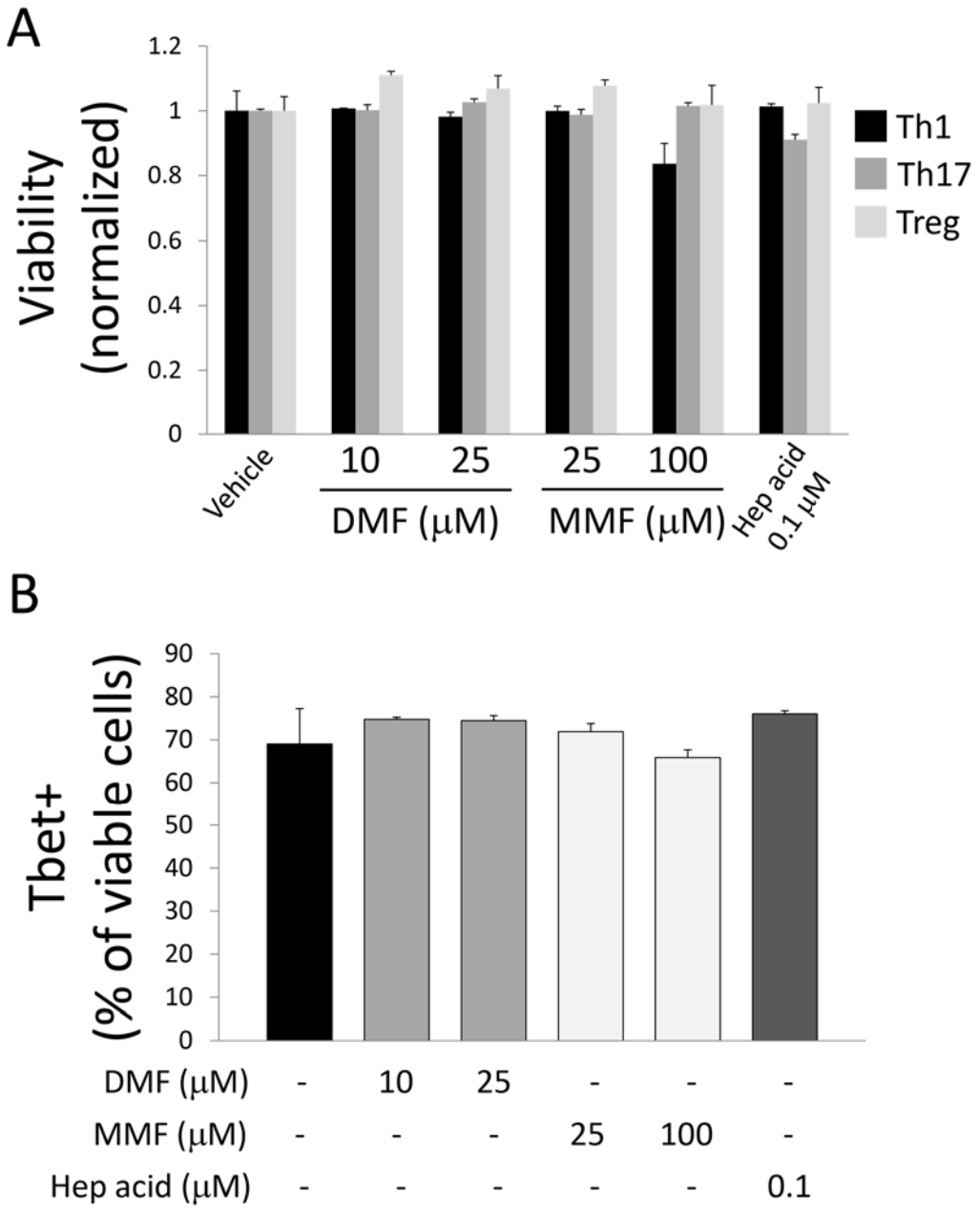

fig. S14. Overnight treatment on day 3 of T–cell polarization has no effect on viability or differentiation. Mouse naïve $CD4^+$ lymphocytes were activated with anti-CD3/CD28 antibodies under Th1–, Th17–, or Treg–cell–polarizing conditions for three days, followed by overnight drug treatment. **(A)** In this paradigm, DMF, MMF, and heptelidic acid had no effect on viability, as assessed by LIVE/DEAD aqua staining. Data represent the mean ± SEM of a triplicate experiment. **(B)** The proportion of $Tbet^+$ cells under Th1–cell–polarizing conditions was unchanged in this paradigm, indicating that differentiation occurred prior to drug treatment. Data represent the mean ± SEM of a triplicate experiment. Results are non-significant by one-way ANOVA.

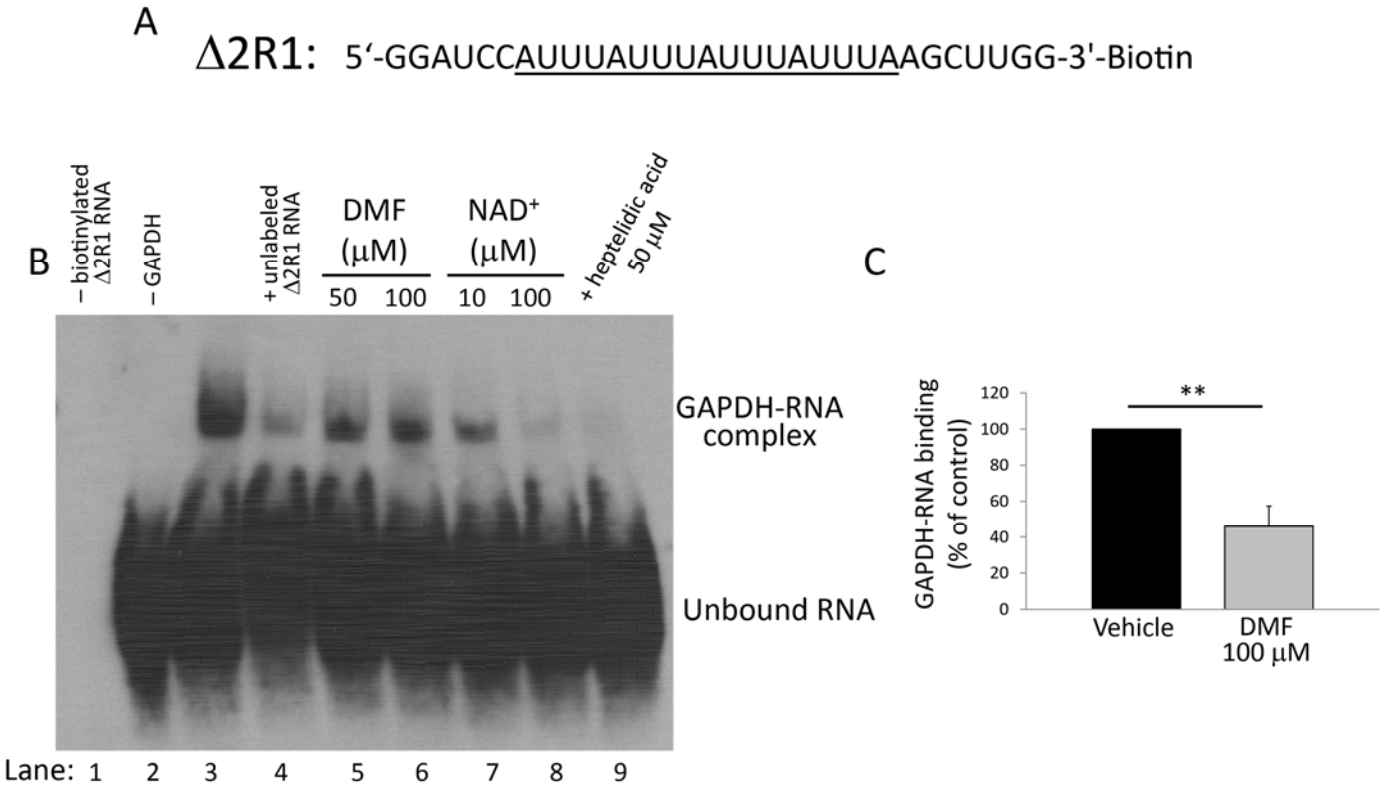

fig. S15. Effect of DMF on GAPDH-RNA binding. (A) Schematic representation of the GAPDH-binding Δ2R1 RNA oligonucleotide, with four AUUUA repeats and a 3' biotin label. **(B)** RNA electrophoretic mobility shift assay (REMSA) demonstrating the relative effects of pre-incubation with DMF, NAD^+, or heptelidic acid on GAPDH binding to biotinylated Δ2R1. Controls: Lane 1: biotinylated Δ2R1 was left out of the binding reaction; Lane 2: GAPDH was left out of the binding reaction; Lane 4: 200–fold excess of unlabeled (non-biotinylated) Δ2R1 was added to the binding reaction to compete with binding to biotinylated Δ2R1. **(C)** Quantification of 100 μM DMF effect on GAPDH-RNA binding. This dose of DMF was chosen because it produces nearly 90% GAPDH inactivation within 30 minutes. Data represent the mean ± SEM of three experiments. $^{**}P < 0.01$ by two-tailed Student's *t* test.

References

1. E. L. Pearce, E. J. Pearce, Metabolic pathways in immune cell activation and quiescence. *Immunity* **38**, 633–643 (2013). doi:10.1016/j.immuni.2013.04.005 Medline

2. B. Kelly, L. A. O'Neill, Metabolic reprogramming in macrophages and dendritic cells in innate immunity. *Cell Res.* **25**, 771–784 (2015). doi:10.1038/cr.2015.68 Medline

3. G. M. Tannahill, A. M. Curtis, J. Adamik, E. M. Palsson-McDermott, A. F. McGettrick, G. Goel, C. Frezza, N. J. Bernard, B. Kelly, N. H. Foley, L. Zheng, A. Gardet, Z. Tong, S. S. Jany, S. C. Corr, M. Haneklaus, B. E. Caffrey, K. Pierce, S. Walmsley, F. C. Beasley, E. Cummins, V. Nizet, M. Whyte, C. T. Taylor, H. Lin, S. L. Masters, E. Gottlieb, V. P. Kelly, C. Clish, P. E. Auron, R. J. Xavier, L. A. J. O'Neill, Succinate is an inflammatory signal that induces IL-1β through HIF-1α. *Nature* **496**, 238–242 (2013). doi:10.1038/nature11986 Medline

4. C. M. Cham, T. F. Gajewski, Glucose availability regulates IFN-γ production and p70S6 kinase activation in $CD8^+$ effector T cells. *J. Immunol.* **174**, 4670–4677 (2005). doi:10.4049/jimmunol.174.8.4670 Medline

5. C. M. Cham, G. Driessens, J. P. O'Keefe, T. F. Gajewski, Glucose deprivation inhibits multiple key gene expression events and effector functions in $CD8^+$ T cells. *Eur. J. Immunol.* **38**, 2438–2450 (2008). doi:10.1002/eji.200838289 Medline

6. R. Wang, C. P. Dillon, L. Z. Shi, S. Milasta, R. Carter, D. Finkelstein, L. L. McCormick, P. Fitzgerald, H. Chi, J. Munger, D. R. Green, The transcription factor Myc controls metabolic reprogramming upon T lymphocyte activation. *Immunity* **35**, 871–882 (2011). doi:10.1016/j.immuni.2011.09.021 Medline

7. A. N. Macintyre, V. A. Gerriets, A. G. Nichols, R. D. Michalek, M. C. Rudolph, D. Deoliveira, S. M. Anderson, E. D. Abel, B. J. Chen, L. P. Hale, J. C. Rathmell, The glucose transporter Glut1 is selectively essential for CD4 T cell activation and effector function. *Cell Metab.* **20**, 61–72 (2014). doi:10.1016/j.cmet.2014.05.004 Medline

8. V. A. Gerriets, R. J. Kishton, A. G. Nichols, A. N. Macintyre, M. Inoue, O. Ilkayeva, P. S. Winter, X. Liu, B. Priyadharshini, M. E. Slawinska, L. Haeberli, C. Huck, L. A. Turka, K. C. Wood, L. P. Hale, P. A. Smith, M. A. Schneider, N. J. MacIver, J. W. Locasale, C. B. Newgard, M. L. Shinohara, J. C. Rathmell, Metabolic programming and PDHK1 control $CD4^+$ T cell subsets and inflammation. *J. Clin. Invest.* **125**, 194–207 (2015). doi:10.1172/JCI76012 Medline

9. C. H. Chang, J. D. Curtis, L. B. Maggi Jr., B. Faubert, A. V. Villarino, D. O'Sullivan, S. C.-C. Huang, G. J. W. van der Windt, J. Blagih, J. Qiu, J. D. Weber, E. J. Pearce, R. G. Jones, E. L. Pearce, Posttranscriptional control of T cell effector function by aerobic glycolysis. *Cell* **153**, 1239–1251 (2013). doi:10.1016/j.cell.2013.05.016 Medline

10. D. Vats, L. Mukundan, J. I. Odegaard, L. Zhang, K. L. Smith, C. R. Morel, R. A. Wagner, D. R. Greaves, P. J. Murray, A. Chawla, Oxidative metabolism and PGC-1β attenuate macrophage-mediated inflammation. *Cell Metab.* **4**, 13–24 (2006). doi:10.1016/j.cmet.2006.05.011 Medline

11. L. Z. Shi, R. Wang, G. Huang, P. Vogel, G. Neale, D. R. Green, H. Chi, HIF1α-dependent glycolytic pathway orchestrates a metabolic checkpoint for the differentiation of T_H17 and T_{reg} cells. *J. Exp. Med.* **208**, 1367–1376 (2011). doi:10.1084/jem.20110278 Medline

12. R. A. Linker, A. Haghikia, Dimethyl fumarate in multiple sclerosis: Latest developments, evidence and place in therapy. *Ther. Adv. Chronic Dis.* **7**, 198–207 (2016). doi:10.1177/2040622316653307 Medline

13. R. A. Linker, D.-H. Lee, S. Ryan, A. M. van Dam, R. Conrad, P. Bista, W. Zeng, X. Hronowsky, A. Buko, S. Chollate, G. Ellrichmann, W. Brück, K. Dawson, S. Goelz, S. Wiese, R. H. Scannevin, M. Lukashev, R. Gold, Fumaric acid esters exert neuroprotective effects in neuroinflammation via activation of the Nrf2 antioxidant pathway. *Brain* **134**, 678–692 (2011). doi:10.1093/brain/awq386 Medline

14. M. M. Blewett, J. Xie, B. W. Zaro, K. M. Backus, A. Altman, J. R. Teijaro, B. F. Cravatt, Chemical proteomic map of dimethyl fumarate-sensitive cysteines in primary human T cells. *Sci. Signal.* **9**, rs10 (2016). doi:10.1126/scisignal.aaf7694 Medline

15. U. Schulze-Topphoff, M. Varrin-Doyer, K. Pekarek, C. M. Spencer, A. Shetty, S. A. Sagan, B. A. C. Cree, R. A. Sobel, B. T. Wipke, L. Steinman, R. H. Scannevin, S. S. Zamvil, Dimethyl fumarate treatment induces adaptive and innate immune modulation independent of Nrf2. *Proc. Natl. Acad. Sci. U.S.A.* **113**, 4777–4782 (2016). doi:10.1073/pnas.1603907113 Medline

16. M. Blatnik, N. Frizzell, S. R. Thorpe, J. W. Baynes, Inactivation of glyceraldehyde-3-phosphate dehydrogenase by fumarate in diabetes: Formation of S-(2-succinyl)cysteine, a novel chemical modification of protein and possible biomarker of mitochondrial stress. *Diabetes* **57**, 41–49 (2008). doi:10.2337/db07-0838 Medline

17. N. H. Litjens, J. Burggraaf, E. van Strijen, C. van Gulpen, H. Mattie, R. C. Schoemaker, J. T. van Dissel, H. B. Thio, P. H. Nibbering, Pharmacokinetics of oral fumarates in healthy subjects. *Br. J. Clin. Pharmacol.* **58**, 429–432 (2004). doi:10.1111/j.1365-2125.2004.02145.x Medline

18. M. Rostami-Yazdi, B. Clement, T. J. Schmidt, D. Schinor, U. Mrowietz, Detection of metabolites of fumaric acid esters in human urine: Implications for their mode of action. *J. Invest. Dermatol.* **129**, 231–234 (2009). doi:10.1038/jid.2008.197 Medline

19. H. Peng, H. Li, A. Sheehy, P. Cullen, N. Allaire, R. H. Scannevin, Dimethyl fumarate alters microglia phenotype and protects neurons against proinflammatory toxic

microenvironments. *J. Neuroimmunol.* **299**, 35–44 (2016). doi:10.1016/j.jneuroim.2016.08.006 Medline

20. Z. D. Parsons, K. S. Gates, Redox regulation of protein tyrosine phosphatases: Methods for kinetic analysis of covalent enzyme inactivation. *Methods Enzymol.* **528**, 129–154 (2013). doi:10.1016/B978-0-12-405881-1.00008-2

21. N. Kamada, S. U. Seo, G. Y. Chen, G. Núñez, Role of the gut microbiota in immunity and inflammatory disease. *Nat. Rev. Immunol.* **13**, 321–335 (2013). doi:10.1038/nri3430 Medline

22. A. A. Shestov, X. Liu, Z. Ser, A. A. Cluntun, Y. P. Hung, L. Huang, D. Kim, A. Le, G. Yellen, J. G. Albeck, J. W. Locasale, Quantitative determinants of aerobic glycolysis identify flux through the enzyme GAPDH as a limiting step. *eLife* **3**, 03342 (2014). Medline

23. M. V. Liberti, Z. Dai, S. E. Wardell, J. A. Baccile, X. Liu, X. Gao, R. Baldi, M. Mehrmohamadi, M. O. Johnson, N. S. Madhukar, A. A. Shestov, I. I. C. Chio, O. Elemento, J. C. Rathmell, F. C. Schroeder, D. P. McDonnell, J. W. Locasale, A predictive model for selective targeting of the Warburg effect through GAPDH inhibition with a natural product. *Cell Metab.* **26**, 648–659.e8 (2017). doi:10.1016/j.cmet.2017.08.017 Medline

24. J. Yun, E. Mullarky, C. Lu, K. N. Bosch, A. Kavalier, K. Rivera, J. Roper, I. I. C. Chio, E. G. Giannopoulou, C. Rago, A. Muley, J. M. Asara, J. Paik, O. Elemento, Z. Chen, D. J. Pappin, L. E. Dow, N. Papadopoulos, S. S. Gross, L. C. Cantley, Vitamin C selectively kills KRAS and BRAF mutant colorectal cancer cells by targeting GAPDH. *Science* **350**, 1391–1396 (2015). doi:10.1126/science.aaa5004 Medline

25. M. A. Michell-Robinson, C. S. Moore, L. M. Healy, L. A. Osso, N. Zorko, V. Grouza, H. Touil, L. Poliquin-Lasnier, A.-M. Trudelle, P. S. Giacomini, A. Bar-Or, J. P. Antel, Effects of fumarates on circulating and CNS myeloid cells in multiple sclerosis. *Ann. Clin. Transl. Neurol.* **3**, 27–41 (2015). doi:10.1002/acn3.270 Medline

26. K. Sakai, K. Hasumi, A. Endo, Identification of koningic acid (heptelidic acid)-modified site in rabbit muscle glyceraldehyde-3-phosphate dehydrogenase. *Biochim. Biophys. Acta* **1077**, 192–196 (1991). doi:10.1016/0167-4838(91)90058-8 Medline

27. E. Nagy, W. F. Rigby, Glyceraldehyde-3-phosphate dehydrogenase selectively binds AU-rich RNA in the NAD^+-binding region (Rossmann fold). *J. Biol. Chem.* **270**, 2755–2763 (1995). doi:10.1074/jbc.270.6.2755 Medline

28. C. M. Spencer, E. C. Crabtree-Hartman, K. Lehmann-Horn, B. A. Cree, S. S. Zamvil, Reduction of $CD8^+$ T lymphocytes in multiple sclerosis patients treated with dimethyl fumarate. *Neurol. Neuroimmunol. Neuroinflamm.* **2**, e76 (2015). doi:10.1212/NXI.0000000000000076 Medline

29. C. C. Gross, A. Schulte-Mecklenbeck, S. Klinsing, A. Posevitz-Fejfár, H. Wiendl, L. Klotz, Dimethyl fumarate treatment alters circulating T helper cell subsets in multiple sclerosis. *Neurol. Neuroimmunol. Neuroinflamm.* **3**, e183 (2015). doi:10.1212/NXI.0000000000000183 Medline

30. M. R. Hara, N. Agrawal, S. F. Kim, M. B. Cascio, M. Fujimuro, Y. Ozeki, M. Takahashi, J. H. Cheah, S. K. Tankou, L. D. Hester, C. D. Ferris, S. D. Hayward, S. H. Snyder, A. Sawa, S-nitrosylated GAPDH initiates apoptotic cell death by nuclear translocation following Siah1 binding. *Nat. Cell Biol.* **7**, 665–674 (2005). doi:10.1038/ncb1268 Medline

31. P. A. Calabresi, R. Allie, K. M. Mullen, S. H. Yun, R. W. Georgantas 3rd, K. A. Whartenby, Kinetics of CCR7 expression differ between primary activation and effector memory states of T_H1 and T_H2 cells. *J. Neuroimmunol.* **139**, 58–65 (2003). doi:10.1016/S0165-5728(03)00127-9 Medline

32. A. Shevchenko, O. N. Jensen, A. V. Podtelejnikov, F. Sagliocco, M. Wilm, O. Vorm, P. Mortensen, A. Shevchenko, H. Boucherie, M. Mann, Linking genome and proteome by mass spectrometry: Large-scale identification of yeast proteins from two dimensional gels. *Proc. Natl. Acad. Sci. U.S.A.* **93**, 14440–14445 (1996). doi:10.1073/pnas.93.25.14440 Medline

33. A. Keller, A. I. Nesvizhskii, E. Kolker, R. Aebersold, Empirical statistical model to estimate the accuracy of peptide identifications made by MS/MS and database search. *Anal. Chem.* **74**, 5383–5392 (2002). doi:10.1021/ac025747h Medline

34. A. I. Nesvizhskii, A. Keller, E. Kolker, R. Aebersold, A statistical model for identifying proteins by tandem mass spectrometry. *Anal. Chem.* **75**, 4646–4658 (2003). doi:10.1021/ac0341261 Medline

35. G. J. van der Windt, C. H. Chang, E. L. Pearce. Measuring bioenergetics in T cells using a Seahorse extracellular flux analyzer. *Curr. Protoc. Immunol.* **113**, 16B.1-16B.14 (2016).

36. V. Vantaku, S. R. Donepudi, C. R. Ambati, F. Jin, V. Putluri, K. Nguyen, K. Rajapakshe, C. Coarfa, V. L. Battula, Y. Lotan, N. Putluri, Expression of ganglioside GD2, reprogram the lipid metabolism and EMT phenotype in bladder cancer. *Oncotarget* **8**, 95620–95631 (2017). doi:10.18632/oncotarget.21038 Medline

37. F. Jin, J. Thaiparambil, S. R. Donepudi, V. Vantaku, D. W. B. Piyarathna, S. Maity, R. Krishnapuram, V. Putluri, F. Gu, P. Purwaha, S. K. Bhowmik, C. R. Ambati, F.-C. von Rundstedt, F. Roghmann, S. Berg, J. Noldus, K. Rajapakshe, D. Gödde, S. Roth, S. Störkel, S. Degener, G. Michailidis, B. A. Kaipparettu, B. Karanam, M. K. Terris, S. M. Kavuri, S. P. Lerner, F. Kheradmand, C. Coarfa, A. Sreekumar, Y. Lotan, R. El-Zein, N. Putluri, Tobacco-specific carcinogens induce hypermethylation, DNA adducts, and DNA

damage in bladder cancer. *Cancer Prev. Res.* **10**, 588–597 (2017). doi:10.1158/1940-6207.CAPR-17-0198 Medline

38. D. W. B. Piyarathna, T. M. Rajendiran, V. Putluri, V. Vantaku, T. Soni, F. C. von Rundstedt, S. R. Donepudi, F. Jin, S. Maity, C. R. Ambati, J. Dong, D. Gödde, S. Roth, S. Störkel, S. Degener, G. Michailidis, S. P. Lerner, S. Pennathur, Y. Lotan, C. Coarfa, A. Sreekumar, N. Putluri, Distinct lipidomic landscapes associated with clinical stages of urothelial cancer of the bladder. *Eur. Urol. Focus* **17**, 30107–30114 (2017). Medline